

## Impact of urban canopy models and external parameters on the modelled urban energy balance in a tropical city

M. Demuzere,<sup>a,b,c\*</sup> S. Harshan,<sup>b</sup> L. Järvi,<sup>d</sup> M. Roth,<sup>b</sup> C. S. B. Grimmond,<sup>e</sup> V. Masson,<sup>f</sup>  
K. W. Oleson,<sup>g</sup> E. Velasco<sup>h</sup> and H. Wouters<sup>a</sup>

<sup>a</sup>Department of Earth and Environmental Sciences, KU Leuven, Belgium

<sup>b</sup>Department of Geography, National University, Singapore

<sup>c</sup>Laboratory of Hydrology and Water Management, Ghent University, Belgium

<sup>d</sup>Department of Physics, University of Helsinki, Finland

<sup>e</sup>Department of Meteorology, University of Reading, UK

<sup>f</sup>CNRM, Météo-France and CNRS, Toulouse, France

<sup>g</sup>National Center for Atmospheric Research, Boulder, CO, USA

<sup>h</sup>Singapore–MIT Alliance for Research and Technology, CENSAM, Singapore

\*Correspondence to: M. Demuzere, KU Leuven, Celestijnenlaan 200E, 3001 Leuven, Belgium.  
E-mail: Matthias.demuzere@kuleuven.be

To date, existing urban land surface models (ULSMs) have been mostly evaluated and optimized for mid- and high-latitude cities. For the first time, we provide a comparative evaluation of four ULSMs for a tropical residential neighbourhood in Singapore using directly measured energy balance components. The simulations are performed offline, for an 11 month period, using the bulk scheme TERRA\_URB and three models of intermediate complexity (CLM, SURFEX and SUEWS). In addition, information from three different parameter lists are used to quantify the impact (interaction) of (between) external parameter settings and model formulations on the modelled urban energy balance components. Encouragingly, overall results indicate good model performance for most energy balance components and align well with previous findings for midlatitude regions, suggesting the transferability of these models to (sub)tropical regions. Similar to results from midlatitude regions, the outgoing long-wave radiation and latent heat flux remain the most problematic fluxes. In addition, the various combinations of models and different parameter values suggest that error statistics tend to be dominated more by the choice of the latter than the choice of model. Finally, our intercomparison framework enabled the attribution of common deficiencies in the different model approaches found previously in midlatitude regions: the simple representation of water intercepted by impervious surfaces leading to a positive bias in the latent heat flux directly after a precipitation event; and the positive bias in modelled outgoing long-wave radiation that is partly due to neglecting the radiative interactions of water vapour between the surface and the tower sensor. These findings suggest that future developments in urban climate research should continue the integration of more physically based processes in urban canopy models, ensure the consistency between the observed and modelled atmospheric properties and focus on the correct representation of urban morphology, water storage and thermal and radiative characteristics.

**Key Words:** urban canopy models; surface energy balance; tropical residential neighbourhood; water vapor opacity; surface interception distribution; local climate zones

Received 19 September 2016; Revised 30 January 2017; Accepted 1 March 2017; Published online in Wiley Online Library 3 May 2017

### 1. Introduction

Cities are hot spots that drive environmental change at multiple scales (Grimm *et al.*, 2008; Georgescu *et al.*, 2014, 2015). As the earth's climate will change over the coming decades (Stocker

*et al.*, 2013), global warming will impact urban areas especially hard, resulting in a major threat to the health and well-being of human populations (Watts *et al.*, 2015). The tendency for urban areas to be warmer than their surrounding rural environments (referred to as the urban heat island) is a well-established

phenomenon and originates from differences in surface energy exchanges over built-up and natural areas (Oke, 1982). A range of urban characteristics (including the high thermal admittance of urban materials, dominance of impervious surfaces – and thus reduced natural pervious surfaces – and the presence of three-dimensional geometries) enhance the absorption of incoming short-wave radiation from the sun and storage of heat energy, partition less energy into evapotranspiration, and reduce a city's ability to cool after sunset, thereby warming the atmosphere nearby.

It is now widely accepted by the climate community that dominant processes leading to local and regional urban warming effects need to be incorporated in climate models. Even though some authors argue that the impact of urban areas might be negligible in terms of temperature and precipitation at coarser spatial resolutions (e.g. >10 km) or depend on the region of interest (Trusilova *et al.*, 2013), others find that e.g. urban expansion implemented at such coarse scales is able to raise near-surface temperatures, not only over the urban areas but also over larger neighbouring areas (Georgescu *et al.*, 2014). Further, the tendency of regional climate modelling towards convection-permitting model scales supports the need for a proper representation of the local city climate (Phelan *et al.*, 2015; Prein *et al.*, 2015). This will allow for an improved assessment of local (urban) climate (projections) as well as the potential for investigating various heat-stress mitigation and adaptation strategies (Prein *et al.*, 2015) such as green urban infrastructure (e.g. Bowler *et al.*, 2010; Demuzere *et al.*, 2014b), water-sensitive urban design (e.g. Coutts *et al.*, 2013) and changing radiative properties of the built environment such as 'cool roofs' (Oleson *et al.*, 2010a; Georgescu *et al.*, 2014).

Cities and their impacts on atmosphere are included in global, regional and local climate models using urban land surface models (ULSMs). A large number of ULSMs are currently available which vary considerably in complexity from simple bulk representations of the surface to more recent developments that consider a complete energy balance at various levels within the urban canyon (Best and Grimmond, 2015). As the first of its kind, (Grimmond *et al.*, 2010) launched the urban land surface model intercomparison project (PILPS-urban) to objectively assess and compare the performance of existing ULSMs. This intercomparison tested a large number of ULSMs (Table 1 in Best and Grimmond, 2015) in offline simulations to evaluate their performance over a light industrial area in Vancouver (British Columbia, Canada) and a suburban area in Melbourne (Australia) (Grimmond *et al.*, 2010, 2011), analysed the representation of the seasonal cycle (Best and Grimmond, 2013) and addressed the role of initial conditions and the response to certain atmospheric conditions (Best and Grimmond, 2014). This effort helped to identify the dominant physical processes, the level of complexity needed in an application specific context, and parameter requirements. Other ULSM evaluations in online mode (coupled to an atmospheric/climate model) include: a single- and a multi-layer urban parametrization within the Coupled Ocean–Atmosphere Mesoscale Prediction System for the New York City metropolitan area (Holt and Pullen, 2007); various urban canopy schemes (slab, single-layer and multi-layer with and without a building energy model) in the Weather Research and Forecasting/Chemistry model to evaluate the regional climate and air quality of the Yangtze River Delta (China) (Liao *et al.*, 2014), and high-resolution regional climate simulations over Berlin (Germany) with the COSMO-CLM regional climate model coupled to the Town Energy Budget (TEB) model (Trusilova *et al.*, 2013, 2015), the Double Canyon Effect Parametrization (DCEP) scheme (Schubert and Grossman-Clarke, 2012) and TERRA\_URB (Wouters *et al.*, 2015, 2016).

In addition to the model physics, the parameters describing the urban surface in terms of land cover, morphology, geometry or radiative and thermal properties play an important role. Ideally

site-specific information about building materials are available, but often generalized global values are used. Regional tables such as Jackson *et al.* (2010) and the ECOCLIMAP data (Champeaux *et al.*, 2005; Faroux *et al.*, 2013) are commonly used by the Community Land Model (Oleson *et al.*, 2008b) or the SURFEX model suite (Masson *et al.*, 2013), respectively. Others have addressed the sensitivity of these parameters via an optimization approach, e.g. by perturbing a set of selected parameters at each step and evaluating how modelled variables evolve. Loridan *et al.* (2010) tested the sensitivity of surface energy fluxes to varying input parameter values for the single-layer urban canopy parametrization used in the Weather Research and Forecasting model, and used this framework to suggest a set of recommended parameter values for three categories of urban areas (Loridan and Grimmond, 2012). Song and Wang (2014) coupled a single-column model to the single-layer urban canopy model SLUCM to address changing urban morphology, albedo, vegetation fraction and aerodynamic roughness on the growth of the atmospheric boundary layer and the distributions of temperature and humidity in the mixed layer under convective conditions. Their results conclude that changes in land-surface properties (hydrothermal or geometric) have a significant impact on the evolution of the overlying boundary layer. In addition, Wouters *et al.* (2016) tested urban canopy parameter value ranges from the Local Climate Zones (Stewart and Oke, 2012) in an online simulation over the Belgian territory with COSMO-CLM coupled to TERRA\_URB. Their study, amongst other results, reveals that, with respect to surface temperatures, air temperatures and associated urban heat islands, one should prioritize those parameters that are most sensitive: the thermal parameters and the anthropogenic heat emissions.

From the above it is clear that off- and online model intercomparisons combined with sensitivity tests related to external parameters are very demanding and also have limitations. Cities are located in vastly different climatic zones and have diverse built-up characteristics (cf. Local Climate Zones; Stewart and Oke, 2012). More research is therefore required for (climate) conditions not addressed in previous studies (Best and Grimmond, 2015). A recent study by Karsisto *et al.* (2016a, 2016b) answered this call and tested the performance of three ULSMs for several sites in and around the high-latitude city of Helsinki (Finland): the Community Land Model (CLM; Lawrence *et al.*, 2011), the Surface Urban Energy and Water Balance Scheme (SUEWS; Järvi *et al.*, 2011, 2014) and SURFEX (Masson *et al.*, 2013). The present study extends this effort by evaluating the three above-mentioned ULSMs together with TERRA\_URB (Wouters *et al.*, 2015, 2016) over a residential neighbourhood in a tropical city. Even though currently most of the rapidly expanding urban areas are located in (sub)tropical regions (Seto *et al.*, 2012), the total number of (sub)tropical urban climate studies is limited Roth (2007). Given that the impact of climate (change) on population health and well-being in these regions has not yet been well established (Kjellstrom and McMichael, 2013; Caminade *et al.*, 2014), it is key to extend the process-based work that seeks to improve our understanding and representation of the (sub)tropical urban climate processes at play (Roth, 2007). Against this background, Singapore's tropical climate provides a unique testbed against which the ULSMs have not yet been bench-marked: a very humid environment with a very small diurnal temperature range. In addition, the selected observation period includes an exceptionally dry two-month period, allowing for an in-depth exploration of the role of precipitation (and the lack thereof) in a tropical setting.

The objective of the present study is to use directly measured energy balance fluxes (Roth *et al.*, 2017; Velasco *et al.*, 2016) to perform model evaluations using three types of input parameter lists. Evaluations are performed for outgoing short- and long-wave radiation ( $K\uparrow$  and  $L\uparrow$  respectively), net all-wave radiation ( $Q^*$ ), turbulent sensible and latent heat fluxes ( $Q_H$  and  $Q_E$  respectively) and the storage heat flux ( $\Delta Q_S$ ). In a first step, the performance of

the models is evaluated for the site-specific reference parameter list. Second, we examine the interaction and sensitivity of all model and parameter list combinations. Finally, the sensitivity of the models with respect to impervious water storage and water vapour opacity is assessed. The article is structured as follows: section 2 provides a brief description of the urban canopy models, the sensitivity studies and evaluation metrics, followed in section 3 by the study site, measurement set-up and description of external parameters. The base-line model evaluation, results of the inter-parameter list and -model interactions as well as the sensitivity experiments are provided in section 4. General findings and recommendations for future work are provided in section 5.

## 2. Methods

Although most models are part of a numerical weather prediction or regional climate model, for the purpose of the present study they are used in an offline mode. They are therefore forced with atmospheric data observed above the canopy layer, which removes a potential source of error produced by the atmospheric model (section 3). For all model simulations, a two-week spin-up period is considered to reduce the influence of model initialization errors. Anthropogenic heat is neglected due to its small contribution to the surface energy balance of the selected site (Quah and Roth, 2012).

### 2.1. Description of urban canopy models

#### 2.1.1. SURFEX

SURFEX combines a range of sub-models able to calculate the exchange of sensible and latent heat, momentum, carbon dioxide and other chemical species, as well as various particles, between the atmosphere and several types of surfaces (Masson *et al.*, 2013). The latter include oceans, inland waters, a large variety of natural land surfaces, and urban areas. Heterogeneity within an area of interest is accounted for by the fractional coverage of each main type (tile) contributing to the total area. Natural tiles are treated by the ISBA (Interaction Soil--Biosphere--Atmosphere) land-surface model. Vegetation is described by the original ISBA evapotranspiration model using an externally imposed leaf area index (also section 3.2). Urban tiles use the TEB model, a single-layer urban canopy model (Masson, 2000). Here, the energy budgets for roofs, walls, and road surfaces are solved separately for a homogeneous isotropic array of street canyons. The lower-boundary conditions for roofs and walls are obtained by prescribing an internal temperature while a zero flux boundary condition is assumed for the road. Although gardens inside street canyons are possible (Lemonsu *et al.*, 2012), in this study vegetated areas are treated as separate tiles with ISBA. The overall structure of TEB is described in more detail in Masson (2000) and Masson *et al.* (2013).

#### 2.1.2. Community Land Model (CLM)

The CLM v4.0 (Bonan *et al.*, 2011; Lawrence *et al.*, 2011) is the land-surface model of the Community Earth System Model (CESM). In CLM, the land surface heterogeneity is represented by main land units (glaciers, lakes, vegetation, wetland and urban), which are further divided into sub-units. The urban fraction, for example, can consist of roof, sunlit and shaded walls, pervious and impervious canyon floor, while vegetation includes representations of up to 17 possible plant functional types. All biogeophysical processes are independently simulated for each sub-unit using the same atmospheric forcing, with subsequent calculation of surface variables and fluxes by averaging the results for individual sub-units and units weighted by their fractional areas (Oleson *et al.*, 2010b). The CLM urban parametrization (CLMU) follows to a large extent the concepts of TEB (section 2.1.1). In CLMU, liquid and solid precipitation can be intercepted, stored and

evaporated from the roof and canyon floor, respectively, while the walls are hydrologically inactive. Recent work by Demuzere *et al.* (2014a) introduced rainwater tanks, biofiltration systems and urban irrigation, while Buzan *et al.* (2015) implemented heat stress metrics. However, these features are not activated in the present study. One of the differences between CLMU and TEB is that in CLMU the roof is coupled to the canyon air properties, while in TEB the roof interacts directly with the canopy air aloft (Demuzere *et al.*, 2013). A more detailed description of CLMU is available in Oleson *et al.* (2008a, 2008b, 2010b).

#### 2.1.3. TERRA\_URB

TERRA\_URB (Wouters *et al.*, 2015, 2016) is the bulk urban land-surface scheme of the COSMO(-CLM) model. It represents the variability of ground heat and moisture transport, the turbulent transfer of momentum, heat and moisture, and the surface--atmosphere radiative exchanges in urban areas. TERRA\_URB has been extensively evaluated in previous studies (Trusilova *et al.*, 2015; Wouters *et al.*, 2015, 2016), demonstrating satisfactory skill in reproducing the different urban surface energy balance components and the urban heat island. It has also been used to consider heat-stress scenarios under future climate and urban land-use change scenarios in Belgium within the Climate Report of the Flemish Environmental Agency (Brouwers *et al.*, 2015). The initial release of TERRA\_URB features the non-iterative calculation of surface-layer stability functions accounting for the roughness sub-layer (Wouters *et al.*, 2012); the impervious water-storage parametrization based on a probability density function of water reservoirs (Wouters *et al.*, 2015); the Semi-empirical Urban canopy dependency parametrization (SURY; Wouters *et al.*, 2016); and the coupling with the turbulence kinetic energy-based surface-layer transfer module of the COSMO(-CLM) model (Doms *et al.*, 2011).

#### 2.1.4. SUEWS

The Surface Urban Energy and Water balance Scheme (SUEWS; Järvi *et al.*, 2011, 2014; Ward *et al.*, 2016) simulates the surface energy and water balance at the neighbourhood scale. It can be run for multiple grids within a city and each model grid is divided into seven surface types including impervious surfaces (buildings and paved), different vegetated surfaces, bare soil and water. The different surfaces are dynamically connected (e.g. water is allowed to move between them). This study uses version SUEWS\_V2016a with an adjusted surface conductance parametrization particularly suitable for non-irrigated urban surfaces (Ward *et al.*, 2016). The radiative flux components are derived from the incoming short-wave solar radiation using the net all-wave radiation scheme (NARP; Offerle *et al.*, 2003; Loridan *et al.*, 2011); the storage heat flux by the objective hysteresis model (OHM; Grimmond *et al.*, 1991); and the latent heat flux uses the Penman--Monteith equation adjusted for urban areas (Grimmond *et al.*, 1991). In contrast to the other models (having  $\Delta Q_S$  as the residual), SUEWS has the sensible heat flux as the residual of the energy balance. The model has been evaluated in offline mode against measurements in several cities (Järvi *et al.*, 2011, 2014; Ward *et al.*, 2016; Karsisto *et al.*, 2016a, 2016b; Alexander *et al.*, 2016b) and used to estimate future climate scenarios in connection with local climate zones (Alexander *et al.*, 2016a; H. C. Ward, 2017; personal communication). It is also part of the Urban Model Evaluation Predictor (Lindberg *et al.*, 2015). Recent developments include an automatic treatment of reanalysis data to be used to force the model (T. Kokkonen, 2016; personal communication).

## 2.2. Impervious water storage

Large differences in evaporation rates between urban and rural environments suggest a strong impact of urbanization on the

global water and energy cycle (Wouters *et al.*, 2015). Evaporation from engineered pavements (e.g. asphalt and concrete) have long been ignored (Nakayama and Fujita, 2010), yet attempts have been made to accurately represent the urban surface water balance, including water storage on impervious surfaces, run-off, evapotranspiration and urban biofiltration and irrigation systems (e.g. Grimmond and Oke, 1991; Masson, 2000; Wang *et al.*, 2013; Demuzere *et al.*, 2014a; De Ridder *et al.*, 2015; Wouters *et al.*, 2015). This study contributes to these ongoing efforts by testing the representation of water-interception reservoirs (puddles) using the Surface Interception Distribution (SID) approach (Wouters *et al.*, 2015), currently embedded in TERRA\_URB. Although this framework was tested for midlatitude sites, Wouters *et al.* (2015) revealed that the annual mean and variability of the surface water balance is very sensitive to these water storage reservoirs. Given that the current study focuses on a tropical site, characterized by an abundance of (intense) precipitation, one can expect an even stronger impact.

The SID approach assumes a linear probability density distribution of water puddles as a function of puddle depth, resulting in the following expression for the evaporative surface fraction (section 2.2 of Wouters *et al.*, 2015, gives a full derivation):

$$\delta = \delta_m \left( \frac{w}{w_m} \right)^{2/3}, \quad (1)$$

where  $\delta_m$  is the maximum puddle fraction,  $w$  is the amount of water in the water puddles, and  $w_m$  is the impervious water-storage capacity. Wouters *et al.* (2015) combined observations from Toulouse (France) and Basel (Switzerland) with model experiments to obtain bulk value estimates yielding  $\delta_m = 0.12 \pm 0.04$  and  $w_m = 1.31 \pm 0.20 \text{ kg m}^{-2}$  (section 3.1 of Wouters *et al.*, 2015). The relation in Eq. (1) is similar to the one used in CLM/SURFEX (e.g. Eq. (48) in Oleson *et al.*, 2008b), although their  $\delta_m = 1$  and  $w_m = 1 \text{ kg m}^{-2}$ . In order to apply Eq. (1) in a single-layer canopy model context for the current site, the TERRA\_URB water-storage parameters are recalculated according to Appendix B in Wouters *et al.* (2015), resulting in  $\delta_m = 0.2$  and  $w_m = 1.31 \text{ kg m}^{-2}$ . To obtain these numbers, two assumptions are made: (i) the walls are hydrologically inactive (default in CLM/SURFEX) and (ii)  $w_m$  is assumed to be identical for roof and road surfaces. In the remainder of this article, this sensitivity run is denoted by ‘SID’.

### 2.3. The water vapour opacity effect

Previous offline evaluations and comparisons for midlatitude sites typically identify a large positive daytime bias in  $L\uparrow$  (e.g. Grimmond *et al.*, 2011; Hénon *et al.*, 2012; Demuzere *et al.*, 2013). Besides other potential explanations (e.g. source areal differences between model and measurement; Järvi *et al.*, 2014) we hypothesize that radiative interactions established by the mixed air in the urban canopy layer is disregarded in the offline set-ups, while being resolved by the atmospheric model in online coupled model set-ups. Such interactions might lead to a poor performance of offline modelled  $L\uparrow$  compared to mast sensor observations located several tens of metres above the urban canopy, for which radiative interactions between the surface and the sensor become important. One of these interactions is the absorption and emission by water vapour (hereafter referred to the water vapour opacity effect, WVO), affecting amongst others the upwelling infrared radiation hitting the sensor at mast height. Infrared radiation emitted from the surface at high temperatures is absorbed by the water vapour molecules. At the same time, the molecules themselves emit infrared radiation at a lower temperature. We hypothesize that these interactions are also relevant for the current site in Singapore: on the one hand – as for any urban site – daytime, and in most cases night-time as well, urban canopy surface temperatures are typically higher than the air temperature aloft (e.g. Coutts *et al.*, 2016; Wouters *et al.*, 2016,

their Figure 2); and tropical regions are characterized by high specific humidity levels (Roth *et al.*, 2017), for which radiative interactions with water vapour may become even more important than for midlatitude sites.

In the absence of hydrometeors, where scattering of infrared radiation can be neglected (Pielke, 2002), the WVO can be approximated as:

$$R^\uparrow(z) \simeq \epsilon(\delta P)\sigma T_a^4 + \{1 - \epsilon(q_v, \delta u)\} L^\uparrow, \quad (2)$$

where  $\epsilon$  is the emissivity (taken as the complement of the transmissivity) as a function of the optical path length  $\delta P = \int_{z_s}^z \rho q_v dz$  between the effective canopy height from where surface radiation originates ( $z_s$ ) and the sensor height ( $z$ ),  $\rho$  is the air density,  $q_v$  is the specific humidity,  $T_a$  is the air temperature and  $\delta u$  is the normal path length between  $z_s$  and  $z$ . For the current study,  $q_v$  and  $T_a$  are approximated by the forcing values (section 3.1) and assumed to be a constant throughout the canopy layer. According to Pielke (2002), the infrared broadband emissivity for water vapour is approximated as:

$$\epsilon(\delta P) = 0.136 \log_{10}(\delta P) + 0.54, \quad \text{for } \log_{10}(\delta P) > 0, \quad (3)$$

with  $\delta P$  expressed in  $\text{g cm}^{-2}$ . More details can be found in Appendix A of Wouters *et al.* (2015).

Since SUEWS directly uses the forcing temperature in order to calculate  $L\uparrow$  (Eq. 11 in Loridan *et al.*, 2011), the effect of the water vapour opacity is only tested for CLM, SURFEX and TERRA\_URB and denoted by ‘WVO’ in the remainder of the article.

### 2.4. Evaluation metrics

Baseline comparison statistics include mean (e.g.  $\bar{X}$ ), standard deviation (e.g.  $\sigma_X$ ), coefficient of determination ( $r^2$ ), mean bias error (MBE), mean absolute error (MAE) and the root mean square error (RMSE) including both its systematic (RMSE<sub>s</sub>) and unsystematic (RMSE<sub>u</sub>) components (e.g. Willmott and Matsuura, 2005; Oleson *et al.*, 2008b; Grimmond *et al.*, 2010; Demuzere *et al.*, 2013). In addition, Taylor diagrams (Taylor, 2001) are used to provide a simultaneous assessment of each model’s capacity to simulate the radiative and turbulent fluxes. Some statistics are normalized by the standard deviation of the observed values (denoted by ‘n’ in front of the statistic’s abbreviation). The significance of the differences between modelled and observed quantities are tested with the Perkins skill score ( $S_{\text{score}}$ ) (e.g. Perkins *et al.*, 2007; Devis *et al.*, 2013, 2014). This simple metric allows for a comparison across probability density functions (PDFs), measuring the common area shared by the modelled and observed PDF. Values range between zero and unity for no and perfect overlap, respectively. In the remainder of this article we consider PDFs to be significantly different when  $S_{\text{score}}$  is  $< 0.8$ , which is more stringent than the value of 0.7 used in Perkins *et al.* (2007) and Devis *et al.* (2013, 2014).

## 3. Site description, measurements and boundary conditions

### 3.1. Telok Kurau measurement site and observations

The data used to force and evaluate the models were measured over a residential neighbourhood of Singapore, which is a small (716 km<sup>2</sup>), densely populated (5.4 million people in 2013), low-lying island city-state located  $\sim 137$  km north of the Equator. The study area in the Telok Kurau (TK) district has low-rise buildings (2–3 storey row and semi-detached houses and a few five-storey condominiums) dissected by a network of mostly minor streets. A detailed site survey covering an area within a 500 m radius around the micrometeorological tower (see below) produced the following morphological and land cover parameters representative of TK (Velasco *et al.*, 2013): an average building and tree height of 9.86 and 7.26 m respectively, a surface cover of 85%

Table 1. Overview of surface cover, morphological, radiative and thermal characteristics describing the residential area of Telok Kurau, Singapore.

		REF	MA03	JA10
Urban fraction (%)	Total	<b>0.85</b>	<b>0.6</b>	<b>0.31</b>
	Buildings	0.39	0.3	0.19
	Pervious roads	–	–	0.04
	Impervious roads	0.46	0.3	0.08
Vegetation fraction (%)	Total	<b>0.15</b>	<b>0.4</b>	<b>0.69</b>
	Evergreen <sup>a</sup>	0.11	0.2	0.37
	Deciduous <sup>a</sup>	–	–	0.09
	C4 grass	0.04	0.2	0.17
	C3 crop	–	–	0.06
Height of roof (m)		9.86	10	30
$H/W$ (–)		0.61	0.21	1.2
$w_m$ (kg m <sup>-2</sup> )		1	1	1
Total thickness (m)	Roof	0.1356	0.55	0.05
	Wall	0.13	0.195	0.34
	Impervious road	1.15	1.15	0.05
Thickness of model layers (m)	Roof	0.05, 0.0006, 0.075, 0.01	0.05, 0.4, 0.1	0.0033 <sup>b</sup>
	Wall	0.01, 0.11, 0.01	0.02, 0.13, 0.05	0.023 <sup>b</sup>
	Impervious road	0.05, 0.1, 1	0.05, 0.1, 1	0.025[exp{0.5(i–0.5)}–1] <sup>c</sup>
$\alpha$ (–)	Bulk	(0.21)	(0.13)	(0.21)
	Roof	0.15	0.15	0.28
	Wall	0.647	0.25	0.25
	Impervious road	0.08	0.08	0.13
$\varepsilon$ (–)	Bulk	(0.92)	(0.91)	(0.87)
	Roof	0.9	0.9	0.82
	Wall	0.9	0.85	0.88
	Impervious road	0.93	0.94	0.91
$C_v$ (MJ m <sup>-3</sup> K <sup>-1</sup> ) <sup>d</sup>	Bulk	(2.65)	(1.38)	(2.39)
	Roof	1.31, 2.37, 0.0012, 1.12	2.11, 2.8, 2.9	1.0
	Wall	1.12, 1.4, 1.12	1.55, 1.55, 2.9	1.01
	Impervious road	2.1, 1.8, 1.5	1.94, 1.28, 1.28	2.06, 1.71
$\lambda$ (W m <sup>-1</sup> K <sup>-1</sup> ) <sup>d</sup>	Bulk	(0.91)	(0.39)	(2.23)
	Roof	0.93, 2.1, 0.026, 0.53	1.51, 0.08, 0.05	0.39
	Wall	0.53, 0.79, 0.53	0.93, 0.93, 0.05	1.38
	Impervious road	2.1, 1.8, 1.5	1.94, 1.28, 1.28	1.67, 0.56

REF is the reference namelist (measured values), MA03 is based on the ECOCLIMAP database used in SURFEX, and JA10 is the generic dataset used in CLMU.

$H/W$  is the canyon height-to-width ratio, and  $w_m$  the maximum water storage on impervious surfaces (roof and impervious road).  $\alpha$ ,  $\varepsilon$ ,  $C_v$  and  $\lambda$  denote albedo, emissivity, volumetric heat capacity and thermal conductivity respectively.

Values in brackets are the bulk values used for TERRA\_URB that are derived from urban-canopy parameters using the Semi-Empirical URban canopy parametrization (SURY; Wouters *et al.*, 2016) – freely available at <https://github.com/hendrikwout/sury> (accessed 27 March 2017).

<sup>a</sup>Broadleaf tropical tree.

<sup>b</sup>The 15 roof and wall layers have a constant thickness.

<sup>c</sup>The impervious road is discretized into 15 layers (denoted by  $i$ ) with an exponentially increasing node depth and thus thickness (Eq. (4.8) in Oleson *et al.*, 2010b).

<sup>d</sup>SUEWS uses the Objective Hysteresis Model (Grimmond *et al.*, 1991). The coefficients used in the current study are  $a_1 = 0.719$  (0.238),  $a_2 = 0.194$  (0.427) and  $a_3 = -36.6$  (–16.7) for impervious surfaces (buildings) (also Järvi *et al.*, 2011).

impervious (39% buildings, 34% gravel/paved, 12% roads) and 15% pervious (11% tree crowns, 4% grass) and an area-averaged height-to-width ratio ( $H/W$ ) of 0.61 (Table 1). Many houses have small gardens covered with turf grass and most streets are lined with shade trees. The area corresponds to LCZ 3 or ‘compact low rise’ (Stewart and Oke, 2012).

A micrometeorological tower installed in the southwest corner of a grass-covered sports field in the centre of the study area (1°18′51.46″N, 103°54′40.31″E; 10 m above sea level) supported various meteorological sensors.

The sensible and latent turbulent energy fluxes were measured using the eddy covariance (EC) technique with a 3D sonic anemometer/infrared gas analyzer (CSAT3/LI-7500; Campbell Scientific, Logan, Utah; LI-COR Biosciences, Lincoln, NE, USA). The up- and downward short- and long-wave fluxes ( $K\uparrow$ ,  $K\downarrow$ ,  $L\uparrow$ ,  $L\downarrow$  respectively) were measured with a four-component net radiometer (CNR1; Kipp & Zonen, Delft, Holland). Additional instrumentation included a temperature/humidity probe ( $T/RH$ ) (HMP45C; Vaisala, Helsinki, Finland). These sensors were installed at a height of 23.7 m to ensure a sufficient height

above the surface roughness to measured spatially representative turbulent fluxes at the neighbourhood scale (e.g. Roth, 2000; Velasco and Roth, 2010). The flux measurements were processed according and subjected to the usual quality control procedures used in EC work. Finally, a rain-gauge (HOBO RG3; Onset Computer Corporation, Bourne, MA, USA) measured rainfall ( $Precip$ ) near the ground. Observed  $\Delta Q_S$  was estimated as the residual from  $Q^*$  and all other terms in the energy balance equation. The TK site and EC measurements have been used in a number of recent urban flux studies and are fully described in Velasco *et al.* (2013) and Roth *et al.* (2017). All models described in section 2.1 are forced with the above-mentioned observations of surface pressure (Pa),  $K\downarrow$ ,  $L\downarrow$  (W m<sup>-2</sup>),  $T$  (K), wind speed (m s<sup>-1</sup>),  $Precip$  (mm h<sup>-1</sup>) and  $RH$  (%).

Because of its equatorial location, Singapore has a typical tropical rainforest climate (Köppen classification Af). Temperature is uniformly high throughout the year (long-term annual mean: 27.5 °C) and rainfall abundant (~2340 mm). The diurnal temperature range is relatively small but larger than the mean month-to-month variability (~6.7 versus  $sim2$  °C respectively).

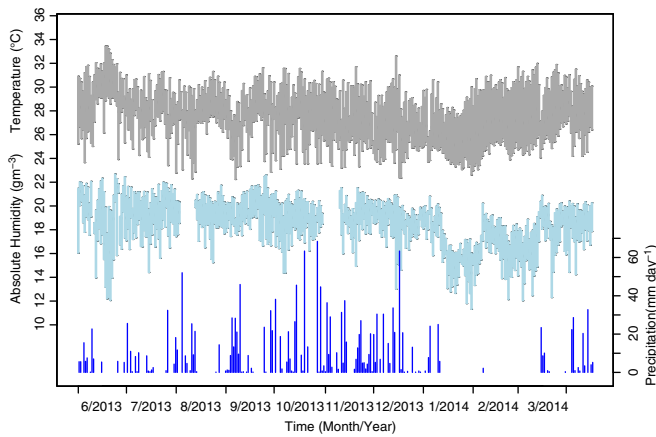


**Figure 1.** Daily temperature (top trace), absolute humidity (middle) and precipitation totals (bottom) for 01 June 2013 to 17 April 2014, observed at Telok Kurau (Singapore). For temperature and humidity, the daily range is indicated by the bars and mean values by the small black symbols. [Colour figure can be viewed at [wileyonlinelibrary.com](http://wileyonlinelibrary.com).]

The climate during the period analysed in the present study (1 June 2013 to 17 April 2014) follows the above-mentioned climate normals, but with one important exception. An unusual dry period occurred from mid-January 2014 to mid-March 2014 during which time only 2.2 mm of rainfall was measured on 8 February 2014 (the long-term monthly rainfall for February is 160 mm). Temperatures (absolute humidities) were slightly above (below) their long-term means for that time of the year (Figure 1).

### 3.2. External parameters

Each land-surface model (including the urban parametrization) is supplied with a specific set of global/regional land-cover characteristics. While these datasets are interchangeable between models, each specific model normally uses a 'native' database.

SURFEX uses the global 1 km ECOCLIMAP database derived from land-cover maps and satellite data (hereafter referred to as MA03) in which each pixel is assigned one of more than 550 land cover types, each associated with a set of parameter values needed by the surface models (Masson *et al.*, 2003). Parameters include the fractional coverage of each main surface type, thermal and radiative characteristics of buildings, walls and roads, and characteristics of the plant functional types (Masson *et al.*, 2013, give details). The 1 km MA03 grid cell size matches that of the source area of the turbulent flux measurements which during daytime (night-time) extends to a maximum of 500 (1000) m (Figures 1 in Velasco *et al.*, 2013; Roth *et al.*, 2017). The MA03 values for the corresponding grid cell is 60% urban, equally divided into buildings and impervious roads. The remainder of the grid cell consists of broadleaf evergreen tropical trees (20%) and C4 grass (20%). The mean building height is 10 m, with a height-to-width ( $H/W$ ) ratio of 0.21. Additional details on the total roof, wall and road thickness, thickness of each individual sub-unit layer and radiative and thermal properties are provided in Table 1.

For CLMU, the urban surface properties are taken from Jackson *et al.* (2010), who provide a global region-specific dataset on urban extent, density, geometry, thermal and radiative characteristics. This is the native generic dataset used for CLMU in global and regional climate studies (e.g. Oleson *et al.*, 2010a, 2013), and is hereafter referred to as JA10. According to this dataset, the urban fraction of the corresponding TK grid cell is  $\sim 31\%$  of which 60% is covered by buildings (roofs), 25% by impervious roads and 15% pervious roads. The vegetation consists mainly of broadleaf evergreen trees with a smaller fraction of broadleaf deciduous trees, C4 grass and C3 crops. The building height and  $H/W$  ratio are 30 m and 1.2, reflecting a higher density urban environment than is actually present (Table 1).

The reference parameter list (hereafter referred to as REF) is compiled to provide the most realistic description of the TK area surrounding the flux tower (section 3.1 and Table 1). The typical building envelope of the low-residential houses in the area was provided by experts of the National University of Singapore, Department of Architecture. The most common wall material is a double brick layer without any cavity and white plaster on the inside and outside. The roofs generally consist of the following four layers: ceramic tiles, aluminium foil, an air gap and plaster. The typical thickness of these layers and the radiative and thermal characteristics (Table 1) for each of the materials are taken from the materials library of the Autodesk Ecotect analysis software (Tools for Sustainability, 2012).

In TERRA\_URB the urban land-cover tile is considered 100% impervious (Wouters *et al.*, 2015). In order to obtain bulk parameter values for roof, wall and road surfaces, the SURY v1.0 parametrization was used to translate facet information from MA03, JA10 and REF to bulk values. Here, the bulk thermal parameter values take into account enhanced ground heat transport and storage due to the increased contact surface expressed by the surface-area index while radiative parameter values consider multiple-facet radiative numerical experiments for calculating the albedo reduction factor resulting from the radiative trapping by the urban canopy (sections 2.1.1 and 2.1.2 respectively in Wouters *et al.*, 2016). The resulting bulk values are indicated in brackets in Table 1. These values are slightly higher than those used in previous applications of TERRA\_URB (Demuzere *et al.*, 2008; De Ridder *et al.*, 2012; Wouters *et al.*, 2015, 2016), but generally fit within the range of LCZ 3 provided in Stewart and Oke (2012).

SUEWS uses the surface cover, morphological (building and tree height) and radiative properties listed in Table 1. Thermal properties for the built-up surfaces are taken into account via the heat storage coefficients used in OHM (Table 1) (Grimmond *et al.*, 1991). For bare soil and vegetated surfaces, the default model values are used (Järvi *et al.*, 2011), except in the calculation of surface conductance where the parameters from Ward *et al.* (2016) are used.

## 4. Results

All models are evaluated using the idealized reference parameter list (REF) (section 4.1); the impact of other external parameter values and their interaction with varying ULSMs is described (section 4.2) and the sensitivity with respect to the impervious water storage and WVO is assessed (section 4.3). Due to the similarity between the CLM and SURFEX models, their results are generally discussed together and referred to as CLM/SURFEX.

### 4.1. Model evaluation using REF parameters

#### 4.1.1. Overall performance

Evaluation metrics using the REF parameter values in Figure 2) are based on 1 h periods using all (day- and night-time) data, except for outgoing short-wave radiation  $K\uparrow$  for which only daytime fluxes ( $K\uparrow > 0 \text{ W m}^{-2}$ ) are used, and all weather conditions. Further details on the statistical values for the simulations using the REF parameter values are provided in Table S1.

Net all-wave radiation ( $Q^*$ ) is well represented by all models, with an  $r^2$  and  $S_{\text{score}}$  close to 1 and a RMSE varying between 16.6 (SUEWS) and 46.1  $\text{W m}^{-2}$  (TERRA\_URB). Most models, except SUEWS, tend to underestimate  $Q^*$  with a maximum MBE of  $-17.3 \text{ W m}^{-2}$  for TERRA\_URB. Although the models are provided with a reference list of external parameters, all models except SUEWS have a  $\text{RMSE}_s$  that is larger than  $\text{RMSE}_u$ , indicating issues with the model physics or the parameters used. The underestimation in  $Q^*$  for CLM/SURFEX and TERRA\_URB is largely driven by an overestimation in outgoing long-wave radiation ( $L\uparrow$ ). The overestimation of  $L\uparrow$  is further compensated

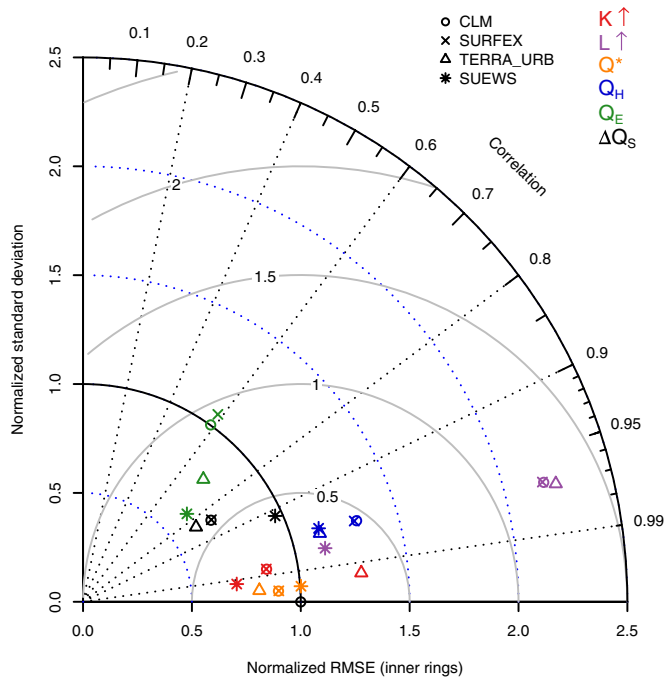


**Figure 2.** Normalized Taylor diagram for four models and six fluxes for the full period using the REF parameter list. Correlation coefficients are plotted on the polar axis, normalized standard deviations on the radial  $y$ -axis and normalized RMSE on the  $x$ -axis (internal circular axes), respectively. [Colour figure can be viewed at [wileyonlinelibrary.com](http://wileyonlinelibrary.com)].

by a slight underestimation of  $K\uparrow$  for all models except TERRA\_URB. For  $Q^*$ ,  $RMSE_s$  is larger than  $RMSE_u$  for both  $K\uparrow$  and  $L\uparrow$  for all models.

Model errors for the turbulent fluxes  $Q_H$ , and especially  $Q_E$ , are larger than the radiative flux component errors. For  $Q_H$ , the  $S_{score}$  of all models is larger than 0.8 while only SUEWS reaches this  $S_{score}$  threshold for  $Q_E$ . (Table S1 and Figure 2). Apart from TERRA\_URB, all models have a positive bias for  $Q_H$ , up to  $9.3 \text{ W m}^{-2}$  for CLM, but for all models,  $RMSE_u$  is larger than  $RMSE_s$ . Model performance is poorest for  $Q_E$  with a maximum  $r^2$  of 0.6 (for SUEWS) and RMSE of  $41.7 \text{ W m}^{-2}$  (SURFEX). The overall magnitude of  $Q_E$  is too low for all models, but the  $RMSE_u$  is always larger than  $RMSE_s$ , except for SUEWS.

Finally, the storage heat flux  $\Delta Q_S$  is best modelled by SUEWS which is surprising since SUEWS uses default values for OHM, not specifically tailored towards the TK site (Table S1 and Figure 2). It is the only model that has a lower systematic than unsystematic RMSE and a  $S_{score}$  above the threshold of 0.8. The other models generally have a too low  $\Delta Q_S$  and  $\sigma$  compared to the observations with a RMSE up to  $64 \text{ W m}^{-2}$  for TERRA\_URB and a negative bias up to  $-7.1 \text{ W m}^{-2}$  for CLM/SURFEX.

#### 4.1.2. Performance during day/night-time and specific weather conditions

After stratifying these result for day/night-time and distinct weather conditions, the largest biases generally occur at night-time, except for  $Q_E$  and  $L\uparrow$  (Figure 3). For the latter, the large RMSE errors for CLM/SURFEX and TERRA\_URB described in section 4.1.1 are mainly due to high daytime RMSE values. In contrast, SUEWS performs better with  $nRMSE = 0.4 \text{ W m}^{-2}/\text{W m}^{-2}$  and similar  $nRMSE_s$  and  $nRMSE_u$  values. The  $nRMSE$  of the latent heat flux is slightly higher during the day than at night, especially for CLM/SURFEX. For all models and fluxes, nighttime  $nRMSE_s$  is larger than  $nRMSE_u$  except for  $L\uparrow$  of SUEWS.

Daytime (night-time) bias is largest for  $L\uparrow$  and  $Q_E$  ( $L\uparrow$ ,  $Q_H$  and  $\Delta Q_S$ ) and all models generally have the same sign. Interestingly, the direction of the bias is opposite between day and night, except for  $Q_E$ , which is underestimated during both parts of

the day. Large differences can be seen for  $L\uparrow$ , being strongly positive during the day and negative during the night, especially for CLM/SURFEX and TERRA\_URB (also section 2.3). This is also reflected in the behaviour of  $Q_H$  and  $\Delta Q_S$ . While during the day too much heat is transported away from the surface via  $Q_H$  instead of being released as  $Q_E$  or stored in the ground, at night too much energy is stored in the ground via  $\Delta Q_S$ , resulting in an underestimation of  $Q_H$ . This is especially true for CLM/SURFEX and TERRA\_URB and less accentuated for SUEWS. It is important to note here that measurement errors are generally larger at night (Best and Grimmond, 2015).

Time series of daily mean MBE for the 11 month period for all models and fluxes are provided in Figure 4. The similarity between CLM and SURFEX causes their time series (red and blue lines) to overlap most of the time. Overall, the skill of all models have a strong temporal variability, although some model/flux combinations tend to maintain similar skill throughout. For example, TERRA\_URB closely follows CLM/SURFEX for  $L\uparrow$  and  $\Delta Q_S$ , while SUEWS often tends to have a very different behaviour. At the start of the dry spell in mid-January, MBE for  $L\uparrow$  drops for SUEWS while it slightly increases for all other models. Simultaneously, the SUEWS bias for  $Q^*$  increases, while it remains at the same level for the other models. Finally, SUEWS has a more strong positive bias during this dry period, which is accompanied by an overestimation of  $\Delta Q_S$ . The prolonged period without precipitation is also accompanied by an observed decrease (increase) in latent (sensible) heat flux. All models are able to capture the slope of this decrease/increase, although the absolute magnitude is underestimated, especially for the latent heat flux.

To further evaluate the model performance under specific weather conditions, the observation period is stratified into a two-month dry period (between 15 January and 15 March 2014) and wet period (15 November 2013 to 14 January 2014) (Figure 5). Notwithstanding a few exceptions, all models perform better during the wet than during the dry conditions. This is especially the case for SUEWS, except for  $L\uparrow$ . All other models have a smaller difference between the dry and wet period for  $K\uparrow$  and  $L\uparrow$ . This is also reflected in the results for  $Q^*$ . The inter-quartile range (IQR) error variability for SUEWS is a lot smaller for  $L\uparrow$  and  $Q^*$ , spanning an error range of approximately  $10 \text{ W m}^{-2}$ , while this is always greater than  $30 \text{ W m}^{-2}$  for the other models.

TERRA\_URB and SUEWS have the best performance for  $Q_H$  for the dry and wet period, with a MBE decreasing from  $-7.8$  and  $-5.8 \text{ W m}^{-2}$  to  $-0.4$  and  $3.7 \text{ W m}^{-2}$ , respectively. For the latent heat flux, the overall negative MBE remains, but is stronger during the dry period than the wet period, even though the magnitude of the flux is smaller during the dry period. This deterioration also occurs in the RMSE components: all models (except SUEWS) have a larger  $RMSE_u$  than  $RMSE_s$ , which is no longer the case during the dry period. The performance of  $\Delta Q_S$  for SUEWS improves significantly during the wet period compared to the dry period. Whereas, CLM/SURFEX and TERRA\_URB have a slight decrease in MBE, but their  $S_{score}$  is better for the wet than the dry period (not shown).

#### 4.1.3. Performance following a precipitation event

The ability of the models to predict the surface--atmosphere exchange following precipitation is investigated using the nMBE as a function of time (hours) since a precipitation event (Figure 6). In total, 72 rainfall events (irrespective of intensity) followed by at least 24 h without precipitation occurred.

For  $K\uparrow$ ,  $Q^*$ ,  $Q_H$  and  $\Delta Q_S$ , the bias is mostly independent of the time since a precipitation event, with an almost constant small positive or negative bias depending on the model or flux of interest (not shown). For  $L\uparrow$  and  $Q_E$ , SUEWS has an almost constant positive and negative bias, respectively, irrespective of the hours since the precipitation event. In contrast for TERRA\_URB, CLM and SURFEX, the nMBE for  $L\uparrow$  more than doubles when

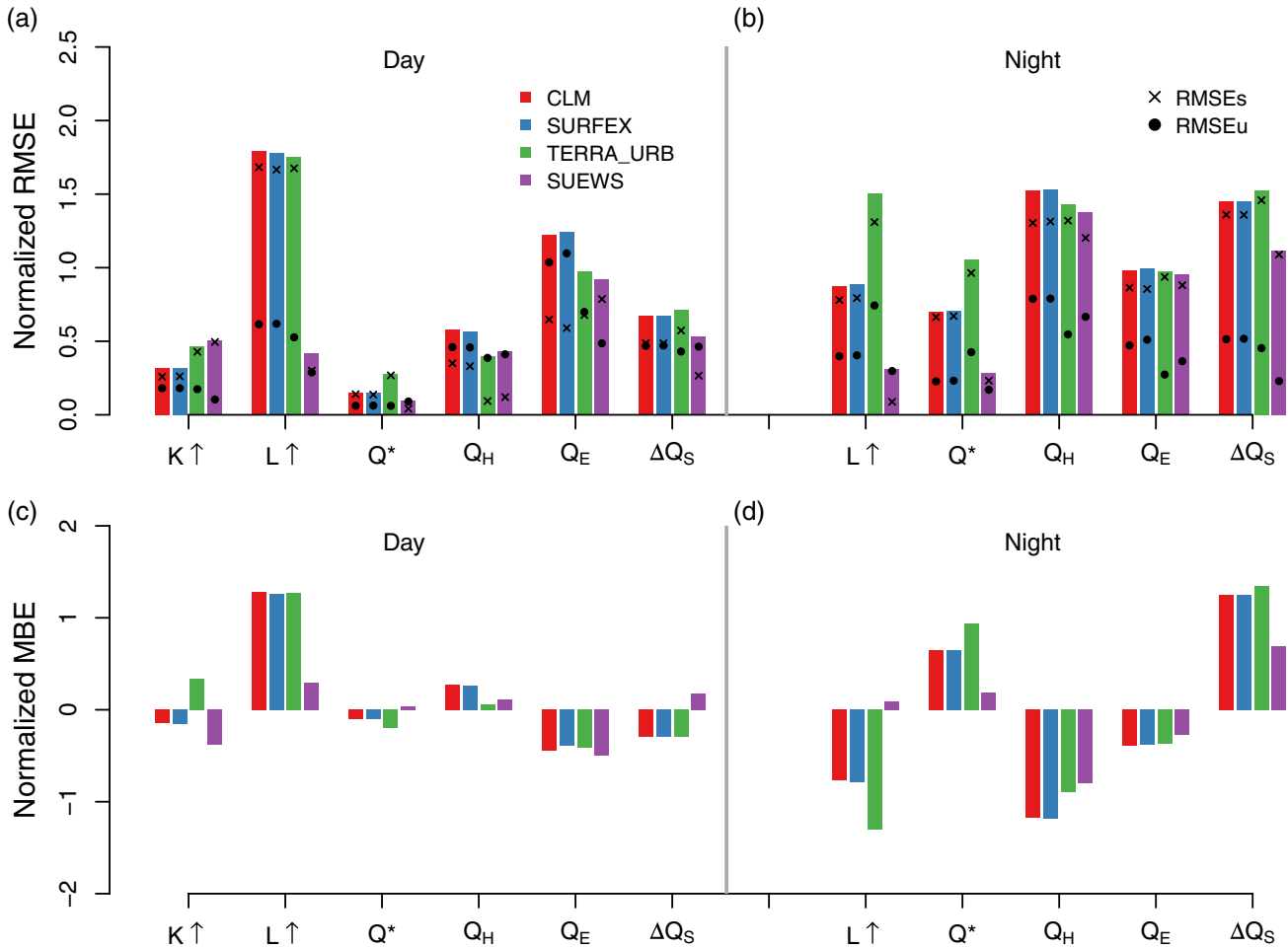


**Figure 3.** Normalized (a, b) RMSE and (c, d) MBE for modelled (a, c) day- and (b, d) night-time fluxes for four models (colours) and the full period using the REF parameter list. Crosses and filled circles in (a, b) are systematic and unsystematic normalized RMSE components, respectively. [Colour figure can be viewed at [wileyonlinelibrary.com](http://wileyonlinelibrary.com)].

comparing their skill directly after, and 24 h after, a rainfall event. For  $Q_E$ , SURFEX and CLM behave similarly, with a peak positive bias 1 h after a precipitation event, reducing to almost  $0 \text{ W m}^{-2}/\text{W m}^{-2}$  after 6 h and further decreasing to a negative normalized bias of  $-0.6 \text{ W m}^{-2}/\text{W m}^{-2}$  after 24 h. Stratifying by accumulated rainfall totals (low, medium, high) in the 24 h leading up to each precipitation event led to a similar relative magnitude and sign of the biases as those in Figure 6 (not shown).

#### 4.2. Inter-parameter list and inter-model variability

The overall influence of using different parameter lists for each model is summarized in Figure 7. Similar to the evaluation of the models using the REF parameter list, CLM and SURFEX behave almost identically when using MA03 and JA10 and they are discussed together. For CLM/SURFEX, altering the parameter list settings to JA10 has the largest impact on  $L\uparrow$  and  $Q_E$ . For  $L\uparrow$ , biases in normalized RMSE and standard deviation are reduced with no change in the correlation coefficient. For  $Q_E$ , the results deteriorate with an increase in nRMSE. This is accompanied by an improvement in correlation and deterioration in variance. Other surface energy balance components are less influenced by changing the parameter list. The results using MA03 are generally within the range of results obtained using REF and JA10.

TERRA\_URB has a similar behaviour as the single-layer canopy models CLM/SURFEX. The error for  $L\uparrow$  decreases when using the JA10 parameter list instead of REF, while the correlation remains constant and the standard deviation improves. Simultaneously, the skill for  $Q_E$  deteriorates, while the underestimated variability in REF is strongly overestimated using JA10. Since the SUEWS model used its own thermal parameters which were not changed between the simulations, this model has the smallest sensitivity to

changes in the parameter list, except for the latent heat flux. For the latter, all skill scores deteriorate with a more than doubling of the nRMSE and a large overestimation of the standard deviation when using JA10. For TERRA\_URB and SUEWS the results for the MA03 parameter list are again between those from REF and JA10 (Figure 7).

To further investigate the parameter list versus inter-model performance, the median and inter-quartile range (IQR) of the hourly biases are analysed (Figure 8) individually for each model and parameter list used. For  $K\uparrow$  (daytime only), all model and parameter list combinations (except JA10 and TERRA\_URB) indicate an underestimation, both in median and IQR (Figures 8(a) and (b)). When using REF, the IQR is smaller than for all other settings ( $\sim 6 \text{ W m}^{-2}$  compared to  $\sim 17 \text{ W m}^{-2}$ , respectively). The underestimation of  $K\uparrow$  contrasts to an overall daytime (night-time) overestimation (underestimation) in  $L\uparrow$ . A large difference between the interquartile ranges can also be noted. During the day it reaches  $\sim 40 \text{ W m}^{-2}$  for the simulations using the REF parameter list (Figure 8(a)), while it is only  $10.6 \text{ W m}^{-2}$  for the SUEWS model using different parameter lists (Figure 8(b)). At night, the differences are smaller with the largest (smallest) median bias and IQR for the JA10 parameter list (SUEWS model) (Figures 8(c) and (d)). The results for both  $K\uparrow$  and  $L\uparrow$  are also reflected in  $Q^*$ . During the day, most parameter list and model combinations underestimate  $Q^*$ , but overestimate during the night. Again, the IQR is smallest for JA10 and SUEWS during day- and night-time.

While the biases for the radiation fluxes are consistent between parameter list and model groups, this is different for daytime turbulent heat fluxes. The overestimation in  $Q_H$  using the REF namelist is converted to an underestimation using JA10. This is compensated by a strong increase in bias and IQR for the latent

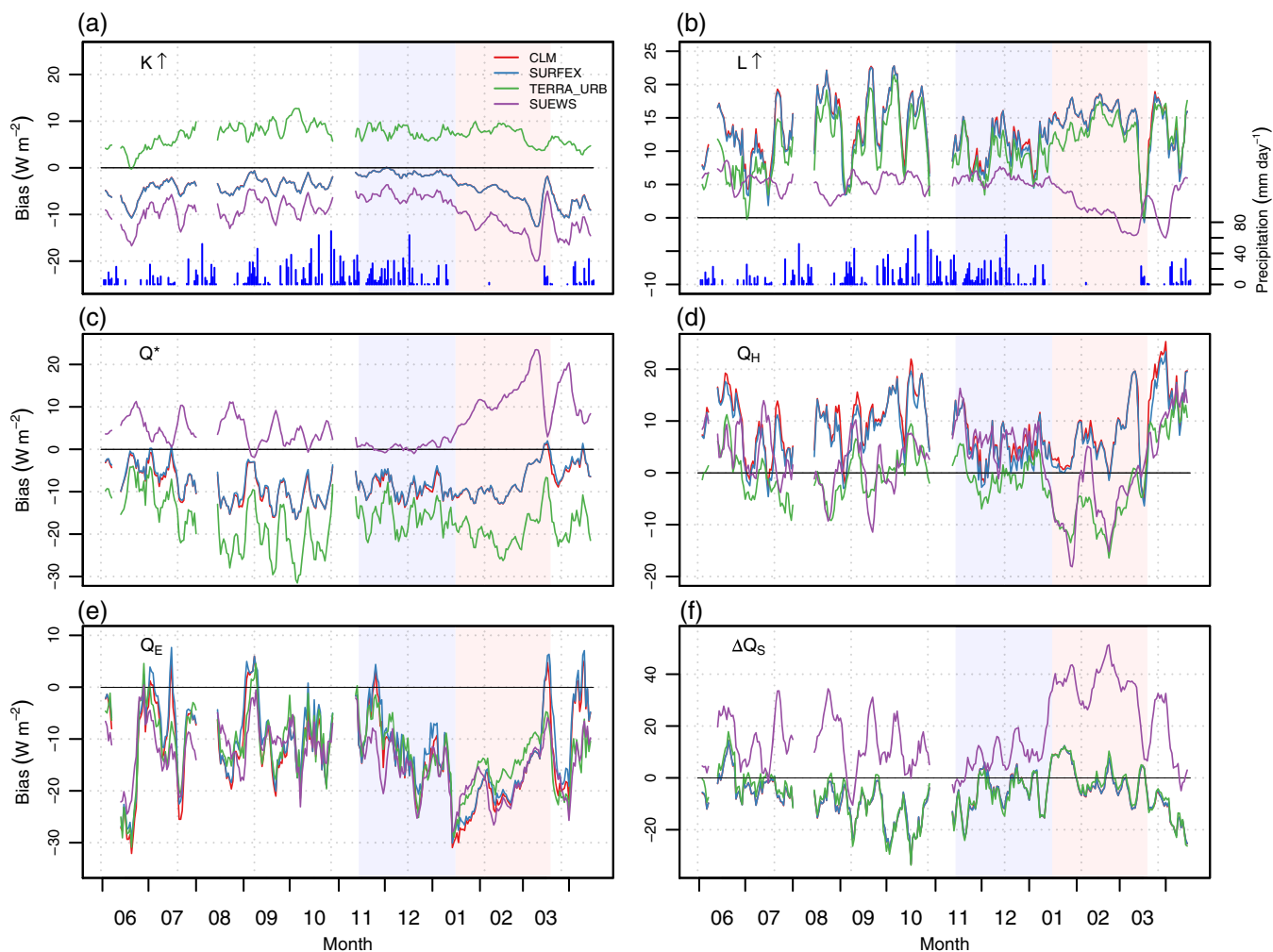


**Figure 4.** Time series of daily mean bias ( $W m^{-2}$ ) for four models (indicated by different colours) and six fluxes ((a) to (f)) for the full period using the REF parameter list. Blue bars in (a, b) are daily precipitation ( $mm day^{-1}$ ). Blue and red shaded areas indicate the selected wet and dry periods, respectively. A 5-day moving average is applied to all time series for clarity. Note different y-axis ranges for different fluxes. Breaks in the time series are periods with missing observations. [Colour figure can be viewed at [wileyonlinelibrary.com](http://wileyonlinelibrary.com)].

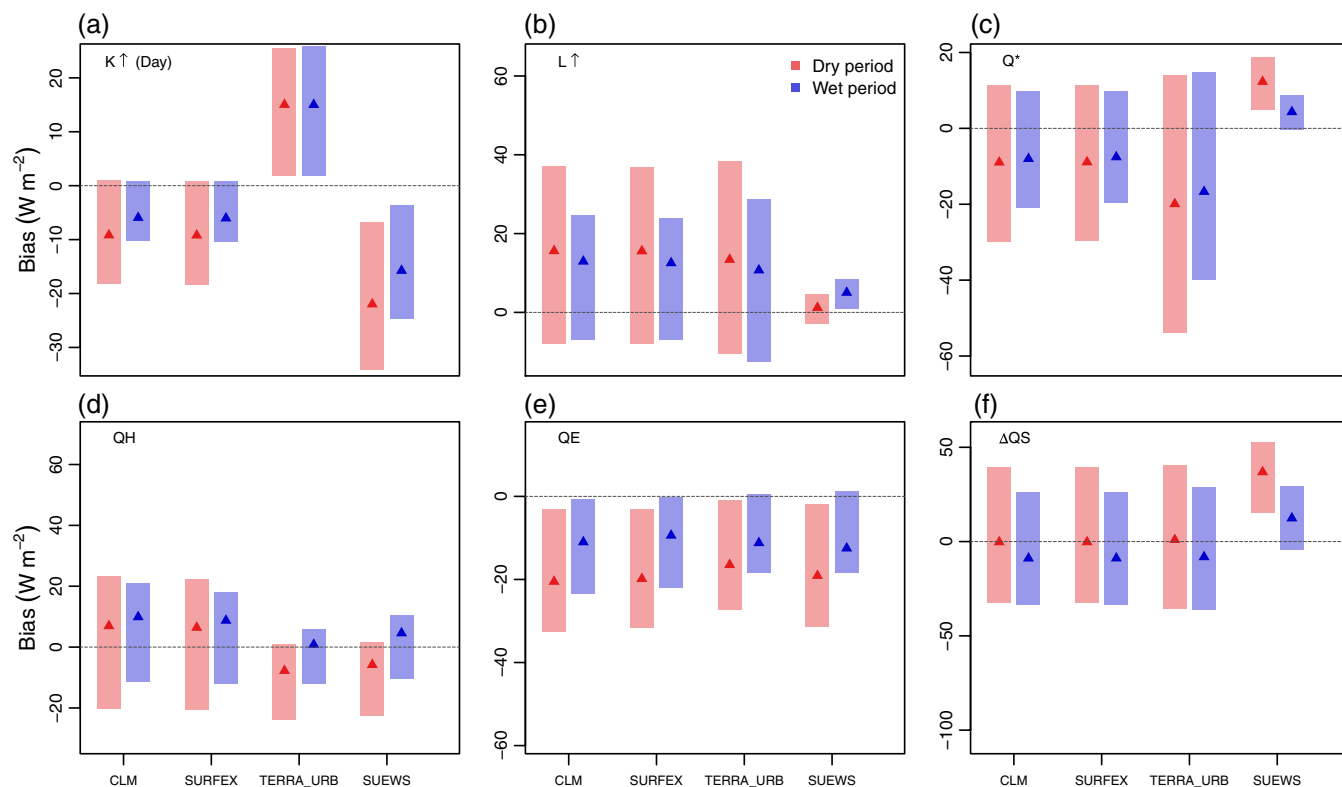


**Figure 5.** Error distribution statistics for six fluxes ((a) to (f)) for the dry (red) and wet (blue) periods for all models using the REF parameter list. Mean values (corresponding to the MBE) and inter-quartile ranges are depicted by dark coloured triangles and light coloured boxes, respectively. For  $K \uparrow$  in (a), only daytime fluxes are used. [Colour figure can be viewed at [wileyonlinelibrary.com](http://wileyonlinelibrary.com)].

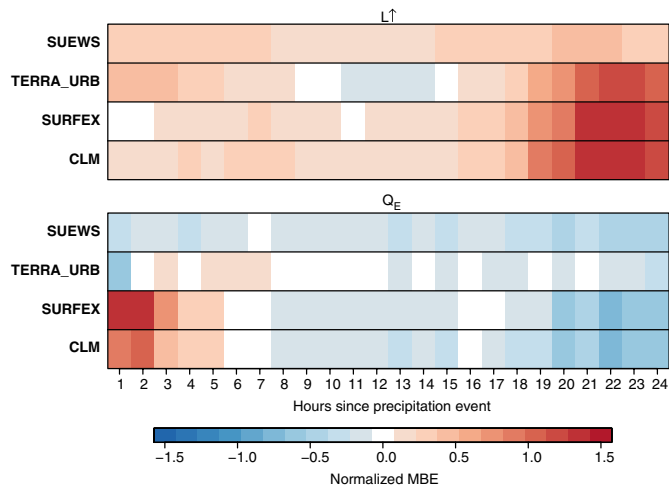


**Figure 6.** Mean normalized bias error for (a)  $L\uparrow$  and (b)  $Q_E$  as a function of time (hours) following a precipitation event for four models for the full period using the REF parameter list ( $\text{W m}^{-2}/\text{W m}^{-2}$ ). Each time bin consists of 72 precipitation events which are identified as having (at least) 24 h without precipitation after the actual precipitation event. [Colour figure can be viewed at [wileyonlinelibrary.com](http://wileyonlinelibrary.com)].

heat flux when moving from REF to JA10 (Figure 8(a)). The results for each model using different parameter lists are more consistent. All models underestimate  $Q_H$  while  $Q_E$  biases are similar but slightly overestimated. During the night, the biases are generally negative and small with a narrow distribution. Best results for night-time  $Q_H$  are obtained with TERRA\_URB, while for  $Q_E$  the bias distribution is almost identical for all models (Figures 8(c) and (d)). Finally, the daytime storage heat flux has a similar bias behaviour across parameter lists and models, generally being underestimated, except for SUEWS. During the night,  $\Delta Q_S$  is most problematic with a median overestimation of at least  $18.5 \text{ W m}^{-2}$  (SUEWS). IQR is also larger than all other fluxes, ranging up to  $24 \text{ W m}^{-2}$  (SUEWS).

Figure 9 confirms that generally the best model results are obtained for  $Q^*$ ,  $K\uparrow$  and  $\Delta Q_S$ , and the worst for  $L\uparrow$  and  $Q_E$  with nMBE values larger than 1. Especially for  $Q_E$  (and to a lesser extent for  $Q_H$  and  $L\uparrow$ ), it is striking that the sign and magnitude of the error depend more on the choice of parameter values rather than choice of model itself. For example, the model results using JA10 strongly overestimate the latent heat flux, while an underestimation is observed when using REF. Here, the best results are obtained for the models using the MA03 parameter list. SUEWS-JA10 ranks best in terms of  $K\uparrow$  but simultaneously performs worst for  $Q_H$  and  $Q_E$ . CLM-MA03 ranks best for  $Q_H$  and  $Q_E$  but performs poorly for  $K\uparrow$ ,  $L\uparrow$  and  $\Delta Q_S$ . In addition, rank numbers for CLM and SURFEX are in most cases only one number apart from each other, which again confirms their similarity noted above (when using the same parameter list settings). Finally, the model, parameter list and their averages do not necessarily perform better than their individual counterparts, although this result is very much dependent on the flux of interest. The simple model averaging solution (same weight for each member, MmPl – Multi-model and Parameter list) provides average rankings from 6 for  $Q^*$  to rank 11 for  $L\uparrow$  and  $Q_H$ . Additional tests using the reliability ensemble averaging (Miao *et al.*, 2014), which uses a weighted average of the ensemble members based on the reliability of its members, did not result in a better ensemble performance (not shown).

#### 4.3. Sensitivity to the treatment of impervious water storage and water vapour opacity

Given the similarity between CLM and SURFEX, the SID framework described in section 2.2 is illustrated for CLM only (note that the SID formulation is already included by default in TERRA\_URB). From Figure 10 it is clear that the

alternative representation of water puddles on the impervious surface has a strong impact on the modelled  $Q_E$ . Both the peak overestimation until 6 h after such a precipitation event as well as the underestimation in the last 6 h of this 24 h period is strongly reduced (compare Figure 10 with Figure 6). In addition, the SID approach positively impacts the full-period error statistics for  $K\uparrow$ ,  $L\uparrow$ ,  $Q_H$  and  $Q_E$ . At the same time, there is a trade-off in skill with a slightly worse performance for  $Q^*$  and  $\Delta Q_S$  (Table S2).

The sensitivity of the modelled  $L\uparrow$  on the effect of WVO is tested for CLM/SURFEX and TERRA\_URB. The error statistics for  $L\uparrow$  (Table S3) compared to the error statistics of the default REF simulations (Table S1) are improved. For all models, the  $S_{\text{score}}$  is larger than 0.9 which is now in line with the default SUEWS model performance. The RMSE is reduced from  $\sim 30$  to  $\sim 5 \text{ W m}^{-2}$ . The large gap between the systematic and unsystematic component of the RMSE in the default setting is now almost negligible for the WVO simulations.

As the WVO effect depends on atmospheric humidity levels, the WVO results are tested for the dry and wet periods discussed in section 4.1.2. During the dry period, the night-time negative bias is completely removed, while the strong daytime overestimation ( $\sim 80 \text{ W m}^{-2}$ ) becomes a small underestimation ( $\sim 10 \text{ W m}^{-2}$ ) (Figure 11(a)). For the wet period, the WVO correction results in a complete removal of the bias throughout the day (Figure 11(b)).

Finally, as the skill of the models in representing  $L\uparrow$  is a function of hours since a precipitation event (Figure 6), the combined effects of SID and WVO are illustrated for CLM in Figure S1. Without taking into account WVO, there is no systematic improvement in modelled  $L\uparrow$ . Introducing WVO has the largest impact and supports the results described above: the modelled  $L\uparrow$  now closely follows the observed  $L\uparrow$  dynamics in the 24 h after the selected rainfall events by removing the positive biases at the beginning and end of this 24 h period. Outside of these 24 h rainfall periods, the SID approach only has a minor effect on the evaporation.

## 5. Discussion and conclusions

The present study provides the first comparative offline evaluation for a tropical residential neighbourhood (Telok Kurau, Singapore) using four urban land surface models. These ULSMs include the bulk scheme TERRA\_URB and three models of intermediate complexity, viz. CLM, SURFEX and SUEWS. All simulations are performed using three different external parameter lists which include the global region-specific Jackson *et al.* (2010) dataset, the ECOCLIMAP database and a reference parameter list derived from expert knowledge and Tools for Sustainability (2012).

The ULSMs under investigation have been evaluated extensively in mid- and high-latitude cities, and are therefore potentially optimized to these regions. Encouragingly, our results using the best available external parameters (REF) align well with previous findings. For example, the second phase of the PILPS-urban project (targeting a suburban site in Melbourne, Australia, characterized by a temperate oceanic climate) found that  $L\uparrow$  is overall not as well modelled as  $K\uparrow$  and that  $Q^*$  is modelled better than either  $K\uparrow$  or  $L\uparrow$  (Grimmond *et al.*, 2011). This is true also for the current model evaluation over Telok Kurau. In addition,  $L\uparrow$  and  $Q_E$  are identified as the most problematic fluxes, which is again in agreement with the findings of the urban intercomparison project PILPS-Urban (Grimmond *et al.*, 2011; Best and Grimmond, 2015).

The performance of varying parameter list and model combinations largely depends on the respective combination and flux of interest. The outgoing long-wave and latent heat fluxes are the most sensitive to changes in the parameter list, but with some exceptions. Since  $L\uparrow$  in SUEWS depends on the forcing temperature  $T$ , the use of a different parameter list has almost no impact. Whereas for the SUEWS  $Q_E$ , the impact of the external parameters is largest (compared to the other models). For all models, using the JA10 parameter list results in strong

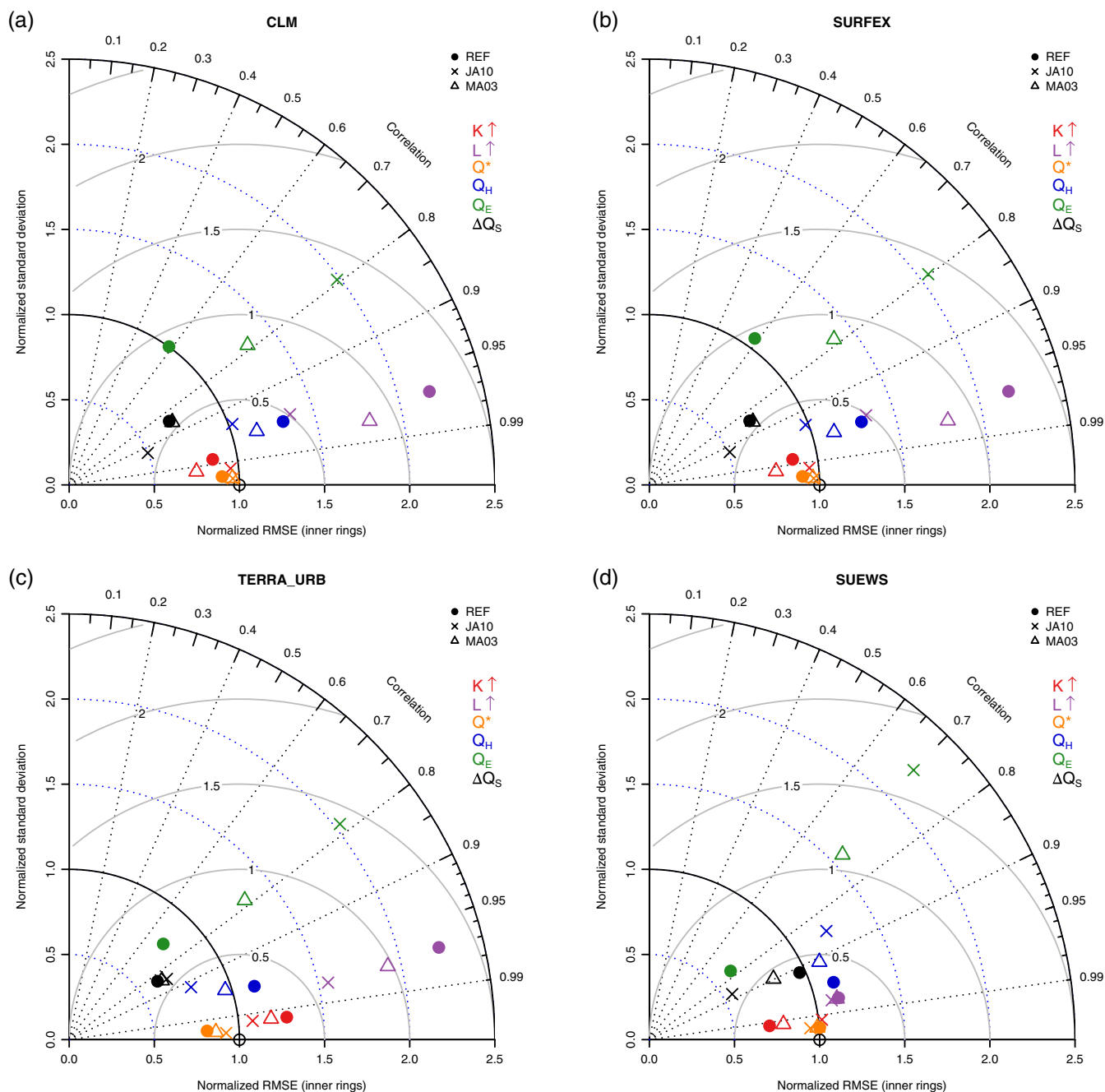


**Figure 7.** As Figure 2, but separately for each model – (a) CLM, (b) SURFEX, (c) TERRA\_URB, and (d) SUEWS – using three parameter lists (indicated by different symbols) as summarized in Table 1. [Colour figure can be viewed at [wileyonlinelibrary.com](http://wileyonlinelibrary.com).]

negative (positive) bias for  $Q_H$  ( $Q_E$ ). The opposite occurs when using the REF parameter list, while using MA03 provides results which are between the former two. The most significant difference between these parameter lists is the amount of urban fraction, which is 30.8, 60 and 85% for JA10, MA03 and REF, respectively. The present results suggest a significant impact of this value but, similar to findings in Loridan and Grimmond (2012), the use of a site-specific urban fraction does not always yield the best model result for  $Q_H$  and  $Q_E$ .

Combining all model and parameter list performances suggests that the error statistics tend to be more dominated by the choice of external parameter values than the choice of model (structure, parametrizations, etc.). For example, the variability between all models driven by one parameter list is often smaller than the variability of one model driven by different parameter lists. Yet, the multi-parameter list and/or multi-model averages do not necessarily outperform each other or the individual realizations, a result, however, that very much depends on the flux of interest. If the focus is on a robust representation of the surface energy balance at an aggregated neighbourhood scale, a simple representation (with a limited

number of parameters) such as TERRA\_URB may be sufficient. Such a scheme is also advantageous in terms of a lower computational cost; bulk parameters are determined beforehand based on detailed radiation model studies, hence avoiding the radiation calculation during the simulation. But, as stated in Best and Grimmond (2015), such representations might not have the physical requirements for more advanced applications such as street-level heat stress studies that benefit from detailed in-canyon radiation information (Buzan *et al.*, 2015).

The humid tropical setting of this residential site together with the exceptional two-month dry period allowed for a more in-depth evaluation of the models' performances during specific weather conditions. First, results vary across models and fluxes considered, but overall their skill deteriorates during dry compared to wet conditions. While this information is valuable in itself, it might have implications for e.g. urban heat island and heat stress studies. Fischer and Schär (2010) and Oleson *et al.* (2015) clearly pointed out that additional heat exacerbates heat stress, morbidity and heat-related mortality, shown to be higher in urban environments during heat waves. Such episodes manifest themselves during heat-wave periods that are generally

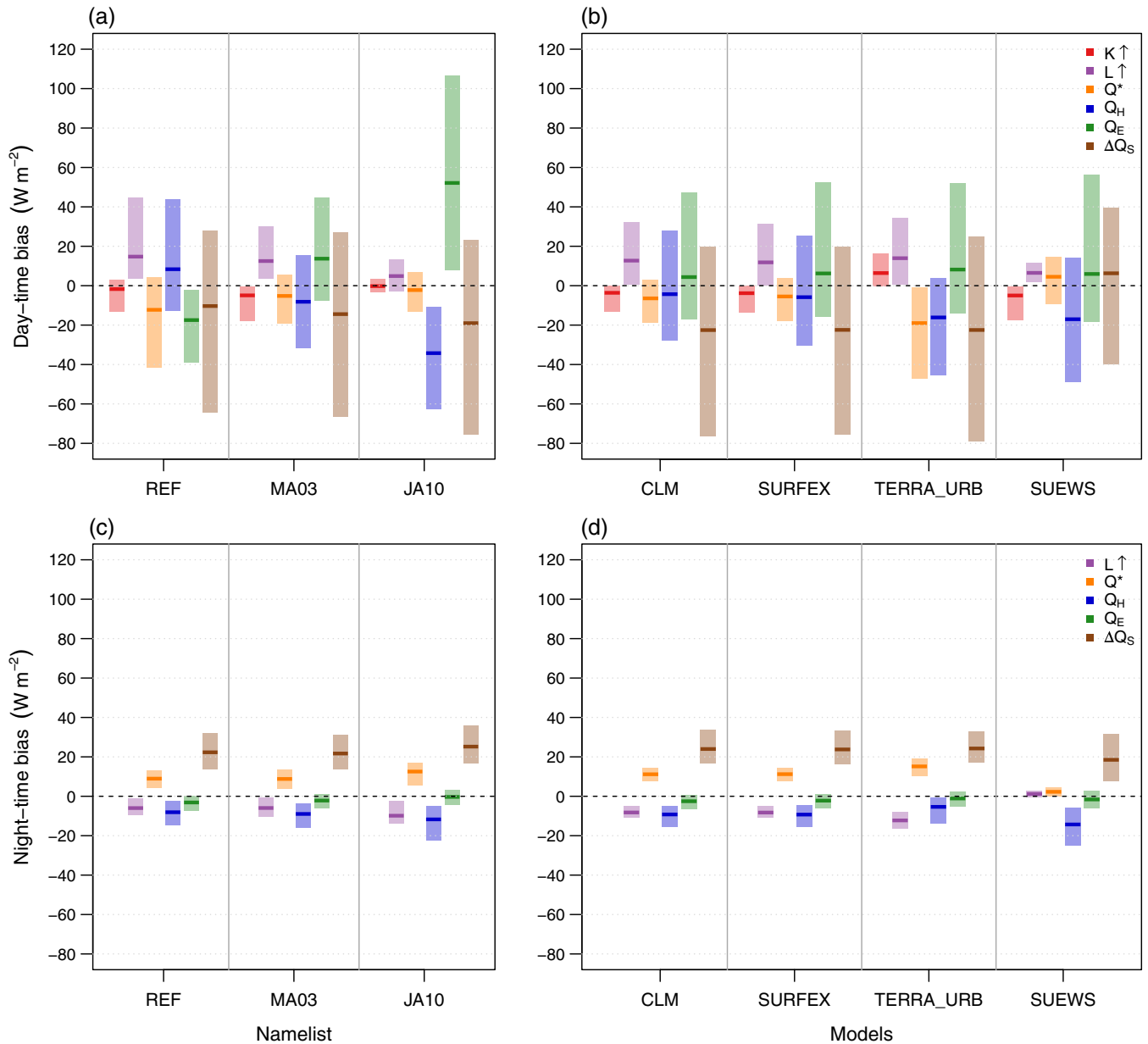


**Figure 8.** Error distribution statistics for (a,b) day and (c,d) night for each parameter list (a,c) over all models and (b,d) for each model over all parameter lists. Different fluxes are indicated by colours, while median values and inter-quartile ranges (IQEs) are depicted by coloured lines and light coloured boxes respectively. e.g. for parameter list REF, all day- and night-time hourly biases over all model runs using REF are combined and the median and IQR of their error distribution are plotted in (a) and (c) for day and night respectively. [Colour figure can be viewed at wileyonlinelibrary.com].

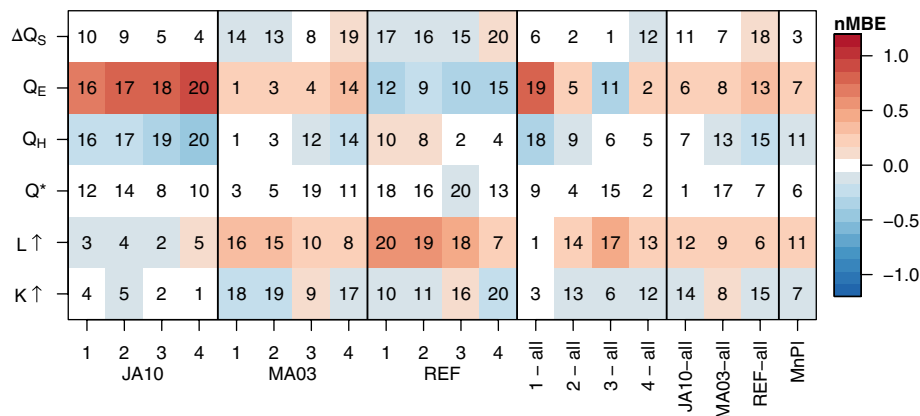


**Figure 9.** Normalized MBE for model and parameter list combinations, as indicated by the colourbar. CLM, SURFEX, TERRA\_URB and SUEWS are referred to as 1, 2, 3 and 4, respectively. The first 12 columns show results for all four models using three parameter lists (JA10, MA03, REF) each. The following four columns show the ensemble average of all three parameter lists for each model, and the next three the ensemble average of all four models for each parameter list. The last column is the average over all model and parameter list combinations (MmPI). The numbers in the matrix are the 'rank' per variable, from 1 (best) to 20 (worst). [Colour figure can be viewed at wileyonlinelibrary.com].

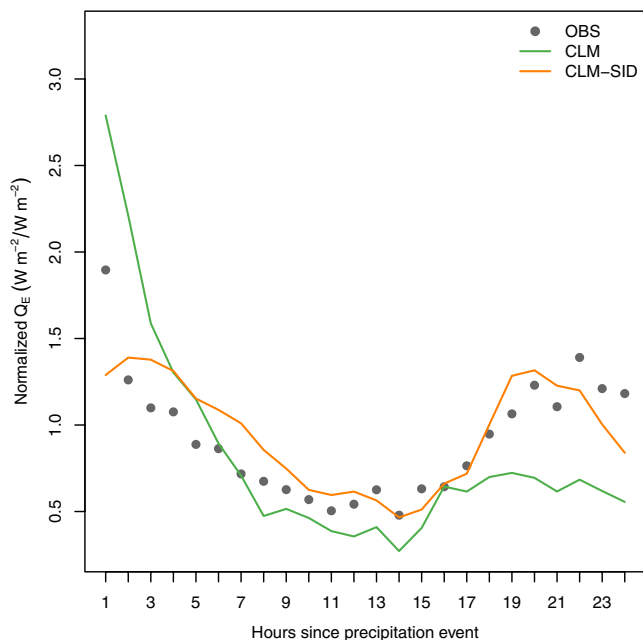


**Figure 10.** Normalized observed and modelled  $Q_E$  as a function of time (hours) following a precipitation event (derived according to Figure 6), for CLM with (CLM-SID) and without (CLM, as in Figure 6) the surface interception distribution approach. [Colour figure can be viewed at [wileyonlinelibrary.com](http://wileyonlinelibrary.com)].

characterized by dry conditions. An inadequate representation of the energy balance components during such events might lead to a misrepresentation of surface and canyon air temperatures (as well as e.g. humidity), in turn leading to incorrect heat stress metrics (e.g. Buzan *et al.*, 2015).

Second, all models reproduce the observed decrease in  $Q_E$  during the exceptional dry period. Yet the magnitude of the modelled latent heat flux is underestimated (stronger during the dry period than in the wet period). When representing the modelled latent heat flux skill as a function of dry hours since a set of precipitation events, SURFEX and CLM show an interesting behaviour: both models overestimate the latent heat flux until 6 h after these events followed by an underestimation in  $Q_E$ . This 'peak' in the first 6 h resembles the peak of the 'PTEB' simulation displayed in Figure 5 of Wouters *et al.* (2015). To address this, the SID approach assuming a depth distribution of water reservoirs on the impervious surface was proposed. This is illustrated in the current study by increasing the maximum water ponding depth  $w_m$  from 1 to 1.31 kg m<sup>-2</sup> and adding a maximal evaporating surface fraction parameter ( $\delta_m = 0.12$ ), as was estimated by Wouters *et al.* (2015). Our results indicate that this framework is both able to alleviate the evaporation peak in the first 6 h after rainfall, as well as the error statistics over the full period. Although the SID and water storage parameters  $w_m$  and  $\delta_m$  were derived and evaluated by Wouters *et al.* (2015) over Toulouse (France) and Basel (Switzerland) respectively, the values are shown to be a good first approximation for tropical Singapore. Given that this approach provides a more physical basis for the maximum water storage  $w_m$  compared to the currently used arbitrary constant of 1 kg m<sup>-2</sup>, it is advised to integrate and further develop the SID framework and the water-storage parameters in future urban model updates.

This finding contributes to the ongoing efforts in improving the often inadequate representation of the urban water budget and the latent heat in ULSMs (Grimmond *et al.*, 2010, 2011). Consequently, this result supports a better assessment of urban adaptation strategies such as e.g. climate- and water-sensitive urban design and green urban infrastructure (Starke *et al.*, 2010; Coutts *et al.*, 2013; Demuzere *et al.*, 2014a, 2014b); and is relevant for improving the performance of numerical meteorological and climate models (Wang *et al.*, 2013; Prein *et al.*, 2015). Especially for tropical (humid) regions, such advancements are critical for a better assessment of e.g. the two-way interaction between

urbanization and the initiation of thunderstorms and their socio-economic consequences (Haberlie *et al.*, 2015; Thiery *et al.*, 2015, 2016).

Third,  $L\uparrow$  results indicate a distinct difference between SUEWS and the three other models. CLM/SURFEX and TERRA\_URB are not only characterized by a large (positive) bias in  $L\uparrow$  during the day turning negative at night, but also by an increasing bias in  $L\uparrow$  during the dry period. In contrast, SUEWS has a small overall bias in  $L\uparrow$  which decreases during the dry period. A reason for this different behaviour can be found in the way the models calculate  $L\uparrow$ . In SUEWS, the radiative flux components are derived from the incoming short-wave solar radiation using the net all-wave radiation scheme (NARP; Loridan *et al.*, 2011). In the latter,  $L\uparrow$  depends on the forcing temperature  $T$  and a correction factor that takes into account the differences between the radiative temperature of the surface and  $T$ . This is clearly different from the other models, in which emitted long-wave radiation is a direct function of modelled surface temperature and emissivity. When these models are evaluated in an offline setting, we hypothesize that neglecting the absorption and emission by water vapour (water vapour opacity effect, WVO) leads to an (artificial) poor representation of modelled  $L\uparrow$  compared to observations from a micrometeorological tower that do register these radiative interactions. This is illustrated in the current study by applying the WVO framework developed by Wouters *et al.* (2015) to TERRA\_URB and CLM/SURFEX. While the REF-driven baseline simulations had a RMSE >30 W m<sup>-2</sup> and  $S_{\text{scores}}$  below 0.7, the simulated  $L\uparrow$  corrected for WVO reduces the RMSE to  $\sim 5$  W m<sup>-2</sup> and  $S_{\text{scores}} > 0.9$ , in line with the results obtained for SUEWS.

All of the above underlines the need to continue our efforts in developing and evaluating ULSMs which can ultimately support the development of urban climate adaptation strategies for (sub)tropical regions (and beyond). When model developments are tested offline using observational datasets, one needs to ensure that there is no mismatch between what is actually measured and modelled (cf. water vapour opacity effect). In addition, future model developments should focus not only on integrating more physically based characteristics in urban canopy models, but also on the correct representation of urban morphology and thermal and radiative characteristics. In terms of urban characteristics, the correct representation of the urban extent, and more specifically the impervious fraction, should be a primary concern when studying the urban impact on the atmosphere at the local, regional or global level. For example, Schneider *et al.* (2010) note an order of magnitude difference between the global urban extent (expressed in km<sup>2</sup>) derived from different global products. In addition, Nordbo *et al.* (2015) emphasize how, within the urban extent, the amount of vegetation also plays a key role in urban climate simulations. In this respect, the 'World Urban Database and Access Portal Tools' (WUDAPT) framework (Bechtel *et al.*, 2015; See *et al.*, 2015) is likely a promising tool. Herein, consistent data are collected at various stages, with level 0 being the Local Climate Zones (LCZs; Stewart and Oke, 2012) and higher level products providing more specific parameters about urban form (canyon height-to-width ratio, building/canyon height), built materials and function. Since the LCZ classifier uses Landsat 8 red, near-infrared and thermal bands, available at 30 m horizontal resolution, the resulting products can be expected to provide a detailed, globally available consistent and comprehensive dataset on the urban landscape with respect to its canopy layer climate (Bechtel *et al.*, 2015; Alexander *et al.*, 2016a).

Finally, future ULSMs evaluations should not only continue for different background climates but also for specific weather conditions within these climates (e.g. Ward *et al.*, 2016). Where possible, the evaluation procedure should aim at an extended multi-variable model approach. Here, the use of e.g. surface temperature measurements either from infrared thermometers or thermal infrared satellite data (e.g. Xu *et al.*, 2008; Parlow *et al.*, 2014; Rayner *et al.*, 2014; Zhao *et al.*, 2014; Wouters *et al.*, 2016) and soil moisture profiles sampled from vegetated or bare soil

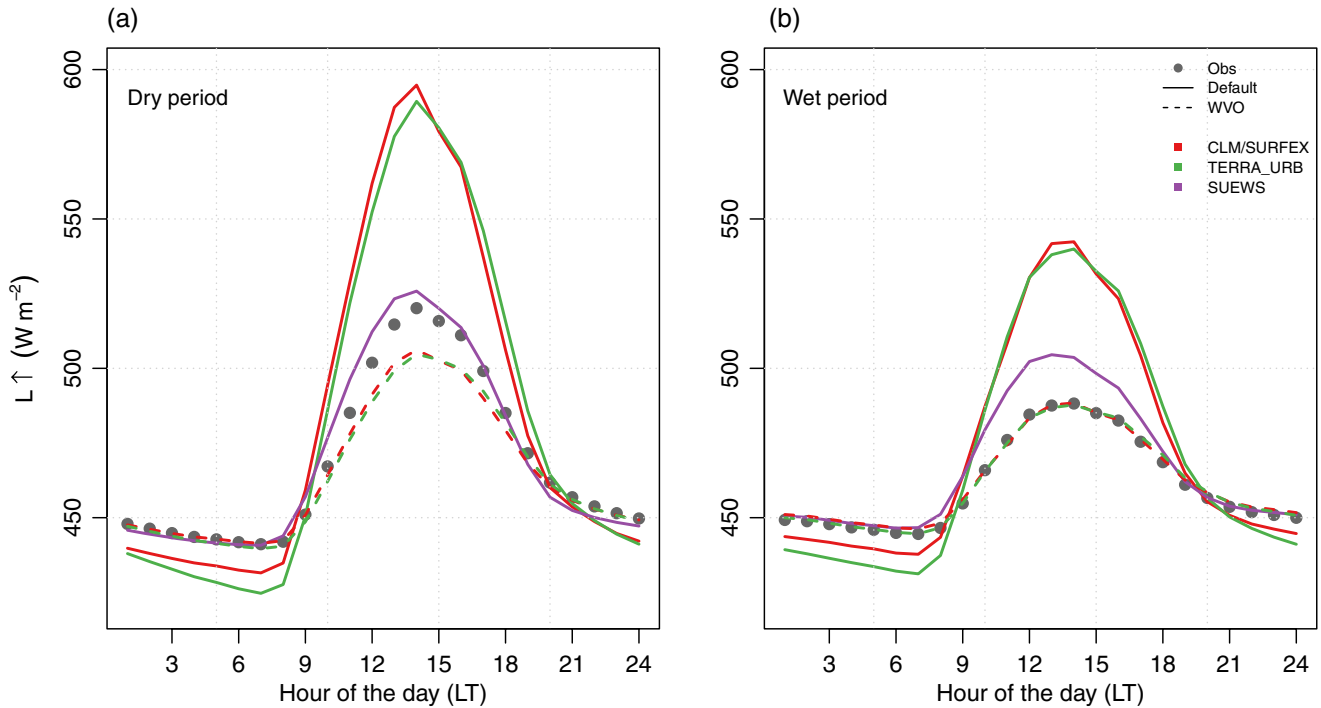


**Figure 11.** Observed and modelled ensemble mean diurnal variation of  $L\uparrow$  for (a) the dry period and (b) the wet period. Full (dashed) lines refer the default model output without (with) accounting for the water vapour opacity framework described in section 2.3. Note that the WVO framework is not relevant for the SUEWS model, but its default output has nevertheless been added for completeness. Because of the similarity between CLM and SURFEX, they are plotted together. [Colour figure can be viewed at [wileyonlinelibrary.com](http://wileyonlinelibrary.com)].

fractions in an urban environment (e.g. Demuzere *et al.*, 2014a) might provide more information about the drivers of error in the modelled surface energy balance components.

#### Acknowledgements

This work has been funded by the Flemish regional government through a FWO (Fund for Scientific Research) post-doctoral position and FWO mobility grant. The model simulations used resources provided by the VSC (Flemish Supercomputer centre), which is funded by the Hercules foundation and the Flemish Government (EWI). We also thank the Academy of Finland (project numbers: 138328, 1127756, ICOS-Finland 281255 and 263149). NCAR is sponsored by the National Science Foundation (NSF). This work also received funding from the Belgian Science Policy Office through its Science for a Sustainable Development Programme under contracts SD/CS/041/MACCBET and BR/143/A2/CORDEX.be. The flux tower operation has been supported by the National Research Foundation Singapore through the Singapore MIT Alliance for Research and Technology's CENSAM research program and the National University of Singapore (research grant R-109-000-091-112). Support from the Met Office/Newton Fund CSSP-China is also acknowledged. Finally, we would like to thank three anonymous reviewers for the insightful and useful comments on an earlier version of this article.

#### Supporting information

The following supporting information is available as part of the online article:

**Figure S1.** Observed and modelled  $L\uparrow$  as a function of time (hours) following a precipitation event. CLM refers to the default version of CLM based on the REF parameter list. CLM-SID, -WVO and -SID-WVO take into account the surface interception distribution, the water vapor opacity effect and both, respectively. **Table S1.** Evaluation metrics for four models and six fluxes using the REF parameters (Table 1) derived from hourly timesteps for the full period. Only daytime data are used for  $K\uparrow$ . Statistics are described in section 2.4. Values in brackets are percentage available observations across the full period.

**Table S2.** As Table S1, but for the CLM model using the surface interception distribution approach (CLM-SID). A better performance for CLM-SID than the default CLM version listed in Table S1 is indicated in bold.

**Table S3.** Evaluation metrics for  $L\uparrow$  for CLM, SURFEX and TERRA\_URB after applying the water vapour opacity framework discussed in section 2.3. All models are driven with the REF parameters (Table 1) and statistics are derived from all hourly timesteps for the full period.

#### References

- Alexander PJ, Bechtel B, Chow WTL, Fealy R, Mills G. 2016a. Linking urban climate classification with an urban energy and water budget model: Multi-site and multi-seasonal evaluation. *Urban Clim.* **17**: 196–215. <https://doi.org/10.1016/j.uclim.2016.08.003>.
- Alexander PJ, Fealy R, Mills GM. 2016b. Simulating the impact of urban development pathways on the local climate: A scenario-based analysis in the greater Dublin region, Ireland. *Landsc. Urban Plan.* **152**: 72–89. <https://doi.org/10.1016/j.landurbplan.2016.02.006>.
- Asefi-Najafabady S, Rayner PJ, Gurney KR, McRobert A, Song Y, Coltin K, Huang J, Elvidge C, Baugh K. 2014. A multiyear, global gridded fossil fuel CO<sub>2</sub> emission data product: Evaluation and analysis of results. *J. Geophys. Res. Atmos.* **119**: 10213–10231. <https://doi.org/10.1002/2013JD021296>.
- Bechtel B, Alexander P, Böhner J, Ching J, Conrad O, Feddema J, Mills G, See L, Stewart I. 2015. Mapping local climate zones for a worldwide database of the form and function of cities. *ISPRS Int. J. Geoinf.* **4**: 199–219. <https://doi.org/10.3390/ijgi4010199>.
- Best MJ, Grimmond CSB. 2013. Analysis of the seasonal cycle within the first international urban land-surface model comparison. *Boundary-Layer Meteorol.* **146**: 421–446. <https://doi.org/10.1007/s10546-012-9769-7>.
- Best MJ, Grimmond CSB. 2014. Importance of initial state and atmospheric conditions for urban land surface models' performance. *Urban Clim.* **10**: 387–406. <https://doi.org/10.1016/j.uclim.2013.10.006>.
- Best MJ, Grimmond CSB. 2015. Key conclusions of the first international urban land surface model comparison project. *Bull. Am. Meteorol. Soc.* **96**: 805–819. <https://doi.org/10.1175/BAMS-D-14-00122.1>.
- Bonan GB, Lawrence PJ, Oleson KW, Levis S, Jung M, Reichstein M, Lawrence DM, Swenson SC. 2011. Improving canopy processes in the Community Land Model version 4 (CLM4) using global flux fields empirically inferred from FLUXNET data. *J. Geophys. Res.* **116**: 1–22. <https://doi.org/10.1029/2010JG001593>.
- Bowler DE, Buyung-Ali L, Knight TM, Pullin AS. 2010. Urban greening to cool towns and cities: A systematic review of the empirical evidence. *Landsc. Urban Plan.* **97**: 147–155. <https://doi.org/10.1016/j.landurbplan.2010.05.006>.
- Brouwers J, Peeters B, Van Steertegem M, van Lipzig N, Wouters H, Beullens J, Demuzere M, Willems P, Ridder KD, Maiheu B, Troch

- RD, Termonia P, Vansteenkiste T, Craninx M, Maetens W, Defloor W, Cauwenberghs K. 2015. *MIRA Climate Report 2015, about Observed and Future Climate Changes in Flanders and Belgium*. Flanders Environment Agency in Collaboration with KU Leuven, VITO and RMI. Flemish Environment Agency – Vlaamse Milieumaatschappij (VMM): Aalst, Belgium. <https://doi.org/10.13140/RG.2.1.2055.8809>.
- Buzan JR, Oleson K, Huber M. 2015. Implementation and comparison of a suite of heat stress metrics within the Community Land Model version 4.5. *Geosci. Model Dev.* **8**: 151–170. <https://doi.org/10.5194/gmd-8-151-2015>.
- Caminade C, Kovats S, Rocklov J, Tompkins AM, Morse AP, Colon-Gonzalez FJ, Stenlund H, Martens P, Lloyd SJ. 2014. Impact of climate change on global malaria distribution. *Proc. Natl. Acad. Sci. U.S.A.* **111**: 3286–3291. <https://doi.org/10.1073/pnas.1302089111>.
- Champeaux JL, Masson V, Chauvin F. 2005. ECOCLIMAP: A global database of land surface parameters at 1 km resolution. *Meteorol. Appl.* **12**: 29–32. <https://doi.org/10.1017/S1350482705001519>.
- Coutts AM, Tapper NJ, Beringer J, Loughnan M, Demuzere M. 2013. Watering our cities: The capacity for water-sensitive urban design to support urban cooling and improve human thermal comfort in the Australian context. *Prog. Phys. Geog.* **37**: 2–28. <https://doi.org/10.1177/0309133312461032>.
- Coutts AM, Harris RJ, Phan T, Livesley SJ, Williams NSG, Tapper NJ. 2016. Thermal infrared remote sensing of urban heat: Hotspots, vegetation, and an assessment of techniques for use in urban planning. *Remote Sens. Environ.* **186**: 637–651. <https://doi.org/10.1016/j.rse.2016.09.007>.
- Demuzere M, De Ridder K, Van Lipzig NPM. 2008. Modeling the energy balance in Marseille: Sensitivity to roughness length parameterizations and thermal admittance. *J. Geophys. Res. Atmos.* **113**: D16120. <https://doi.org/10.1029/2007JD009113>.
- Demuzere M, Oleson K, Coutts AM, Pigeon G, van Lipzig NPM. 2013. Simulating the surface energy balance over two contrasting urban environments using the Community Land Model Urban. *Int. J. Climatol.* **33**: 3182–3205. <https://doi.org/10.1002/joc.3656>.
- Demuzere M, Coutts AM, Göhler M, Broadbent AM, Wouters H, van Lipzig NPM, Gebert L. 2014a. The implementation of biofiltration systems, rainwater tanks and urban irrigation in a single-layer urban canopy model. *Urban Clim.* **10**: 148–170. <https://doi.org/10.1016/j.uclim.2014.10.012>.
- Demuzere M, Orru K, Heidrich O, Olazabal E, Geneletti D, Orru H, Bhave AG, Mittal N, Feliu E, Faehnle M. 2014b. Mitigating and adapting to climate change: Multi-functional and multi-scale assessment of green urban infrastructure. *J. Environ. Manag.* **146**: 107–115. <https://doi.org/10.1016/j.jenvman.2014.07.025>.
- De Ridder K, Bertrand C, Casanova G, Lefebvre W. 2012. Exploring a new method for the retrieval of urban thermophysical properties using thermal infrared remote sensing and deterministic modeling. *J. Geophys. Res. Atmos.* **117**: D17108. <https://doi.org/10.1029/2011JD017194>.
- De Ridder K, Lauwaet D, Maiheu B. 2015. UrbClim – A fast urban boundary layer climate model. *Urban Clim.* **12**: 21–48. <https://doi.org/10.1016/j.uclim.2015.01.001>.
- Devis A, Van Lipzig NPM, Demuzere M. 2013. A new statistical approach to downscale wind speed distributions at a site in northern Europe. *J. Geophys. Res. Atmos.* **118**: 2272–2283. <https://doi.org/10.1002/jgrd.50245>.
- Devis A, Van Lipzig NPM, Demuzere M. 2014. A height-dependent evaluation of wind and temperature over Europe in the CMIP5 earth system models. *Clim. Res.* **61**: 41–56. <https://doi.org/10.3354/cr01242>.
- Doms G, Förstner J, Heise E, Herzog HJ, Mironov D, Raschendorfer M, Reinhardt T, Ritter B, Schrodin R, Schulz JP, Vogel G. 2011. 'Consortium for small-scale modelling. A description of the non-hydrostatic regional COSMO model. Part II: Physical parameterization', Technical report LM F90 4.20. COSMO. <http://www.cosmo-model.org/content/model/documentation/core/cosmoPhysParamtr.pdf> (accessed 28 March 2017).
- Faroux S, Kaptué Tchuenté AT, Roujean JL, Masson V, Martin E, Le Moigne P. 2013. ECOCLIMAP-II/Europe: A twofold database of ecosystems and surface parameters at 1 km resolution based on satellite information for use in land surface, meteorological and climate models. *Geosci. Model Dev.* **6**: 563–582. <https://doi.org/10.5194/gmdd-5-563-2012>.
- Fischer EM, Schär C. 2010. Consistent geographical patterns of changes in high-impact European heatwaves. *Nat. Geosci.* **3**: 398–403. <https://doi.org/10.1038/ngeo866>.
- Georgescu M, Morefield PE, Bierwagen BG, Weaver CP. 2014. Urban adaptation can roll back warming of emerging megapolitan regions. *Proc. Natl. Acad. Sci. U.S.A.* **111**: 2909–2914. <https://doi.org/10.1073/pnas.1322280111>.
- Georgescu M, Chow WTL, Wang ZH, Brazel A, Trapido-Lurie B, Roth M, Benson-Lira V. 2015. Prioritizing urban sustainability solutions: Coordinated approaches must incorporate scale-dependent built environment induced effects. *Environ. Res. Lett.* **10**: 061001. <https://doi.org/10.1088/1748-9326/10/6/061001>.
- Grimm NB, Faeth SH, Golubiewski NE, Redman CL, Wu J, Bai X, Briggs JM, Grimm NB, Faeth SH, Golubiewski NE, Redman CL, Wu J, Bal X, Briggs JM. 2008. Global change and the ecology of cities. *Science* **319**: 756–760. <https://doi.org/10.1126/science.1150195>.
- Grimmond CSB, Oke TR. 1991. An evapotranspiration-interception model for urban areas. *Water Resour. Res.* **27**: 1739–1755. <https://doi.org/10.1029/91WR00557>.
- Grimmond CSB, Cleugh H, Oke TR. 1991. An objective urban heat storage model and its comparison with other schemes. *Atmos. Environ.* **25**: 311–326. [https://doi.org/10.1016/0957-1272\(91\)90003-W](https://doi.org/10.1016/0957-1272(91)90003-W).
- Grimmond CSB, Blackett M, Best MJ, Barlow J, Baik JJ, Belcher SE, Bohnenstengel SI, Calmet I, Chen F, Dandou A, Fortuniak K, Gouvea ML, Hamdi R, Hendry M, Kawai T, Kawamoto Y, Kondo H, Krayenhoff ES, Lee SH, Loridan T, Martilli A, Masson V, Miao S, Oleson K, Pigeon G, Porson A, Ryu YH, Salamanca F, Shashua-Bar L, Steeneveld GJ, Tombrou M, Voogt J, Voogt D, Zhang N. 2010. The international urban energy balance models comparison project: First results from phase 1. *J. Appl. Meteorol. Climatol.* **49**: 1268–1292. <https://doi.org/10.1175/2010JAMC2354.1>.
- Grimmond CSB, Blackett M, Best MJ, Baik JJ, Belcher SE, Beringer J, Bohnenstengel SI, Calmet I, Chen F, Coutts A, Dandou A, Fortuniak K, Gouvea ML, Hamdi R, Hendry M, Kanda M, Kawai T, Kawamoto Y, Kondo H, Krayenhoff ES, Lee SH, Loridan T, Martilli A, Masson V, Miao S, Oleson K, Ooka R, Pigeon G, Porson A, Ryu YH, Salamanca F, Steeneveld GJ, Tombrou M, Voogt JA, Young DT, Zhang N. 2011. Initial results from Phase 2 of the international urban energy balance model comparison. *Int. J. Climatol.* **31**: 244–272. <https://doi.org/10.1002/joc.2227>.
- Haberlie A, Ashley W, Pingel T. 2015. The effect of urbanisation on the climatology of thunderstorm initiation. *Q. J. R. Meteorol. Soc.* **141**: 663–675. <https://doi.org/10.1002/qj.2499>.
- Hénon A, Mestayer PG, Lagouarde JP, Voogt JA. 2012. An urban neighborhood temperature and energy study from the CAPITOUL experiment with the Solene model. Part 2: Influence of building surface heterogeneities. *Theor. Appl. Climatol.* **110**: 197–208. <https://doi.org/10.1007/s00704-012-0616-z>.
- Holt T, Pullen J. 2007. Urban canopy modeling of the New York City metropolitan area: A comparison and validation of single- and multilayer parameterizations. *Mon. Weather Rev.* **135**: 1906–1930. <https://doi.org/10.1175/MWR3372.1>.
- Jackson TL, Feddema JJ, Oleson KW, Bonan GB, Bauer JT. 2010. Parameterization of urban characteristics for global climate modeling. *Ann. Assoc. Am. Geogr.* **100**: 848–865. <https://doi.org/10.1080/00045608.2010.497328>.
- Järvi L, Grimmond CSB, Christen A. 2011. The Surface Urban Energy and Water Balance Scheme (SUEWS): Evaluation in Los Angeles and Vancouver. *J. Hydrol.* **411**: 219–237. <https://doi.org/10.1016/j.jhydrol.2011.10.001>.
- Järvi L, Grimmond CSB, Taka M, Nordbo A, Setälä H, Strachan IB. 2014. Development of the Surface Urban Energy and Water Balance Scheme (SUEWS) for cold climate cities. *Geosci. Model Dev.* **7**: 1691–1711. <https://doi.org/10.5194/gmd-7-1691-2014>.
- Karsisto P, Fortelius C, Demuzere M, Grimmond CSB, Oleson KW, Kouznetsov R, Masson V, Järvi L. 2016a. Seasonal surface urban energy balance and wintertime stability simulated using three land-surface models in the high-latitude city Helsinki. *Q. J. R. Meteorol. Soc.* **142**: 401–417. <https://doi.org/10.1002/qj.2659>.
- Karsisto P, Fortelius C, Demuzere M, Grimmond CSB, Oleson KW, Kouznetsov R, Masson V, Järvi L. 2016b. Seasonal surface urban energy balance and wintertime stability simulated using three land-surface models in the high-latitude city Helsinki. *Q. J. R. Meteorol. Soc.* **142**: 401–417.
- Kjellstrom T, McMichael AJ. 2013. Climate change threats to population health and well-being: The imperative of protective solutions that will last. *Global Health Action* **6**: 1–9. <https://doi.org/10.3402/gha.v6i0.20816>.
- Lawrence DM, Oleson KW, Flanner MG, Thornton PE, Swenson SC, Lawrence PJ, Zeng X, Yang ZL, Levis S, Sakaguchi K, Bonan GB, Slater AG. 2011. Parameterization improvements and functional and structural advances in version 4 of the Community Land Model. *J. Adv. Model. Earth Syst.* **3**: 1–27. <https://doi.org/10.1029/2011MS000045>.
- Lemonsu A, Masson V, Shashua-Bar L, Erel E, Pearlmutter D. 2012. Inclusion of vegetation in the town energy balance model for modelling urban green areas. *Geosci. Model Dev.* **5**: 1377–1393. <https://doi.org/10.5194/gmd-5-1377-2012>.
- Liao J, Wang T, Wang X, Xie M, Jiang Z, Huang X, Zhu J. 2014. Impacts of different urban canopy schemes in WRF/Chem on regional climate and air quality in Yangtze River Delta, China. *Atmos. Res.* **145–146**: 226–243. <https://doi.org/10.1016/j.atmosres.2014.04.005>.
- Lindberg F, Grimmond CSB, Onomura S, Järvi L, Ward H. 2015. 'UMEPan integrated tool for urban climatology and climate-sensitive planning applications'. In ICUC 99th International Conference on Urban Climate Jointly with 12th Symposium on the Urban Environment, TUKUP7 (cont): Warning Plans & Decision Support Tools. Toulouse, France.
- Loridan T, Grimmond CSB. 2012. Multi-site evaluation of an urban land-surface model: Intra-urban heterogeneity, seasonality and parameter complexity requirements. *Q. J. R. Meteorol. Soc.* **138**: 1094–1113. <https://doi.org/10.1002/qj.963>.
- Loridan T, Grimmond CSB, Grossman-Clarke S, Chen F, Tewari M, Manning K, Martilli A, Kusaka H, Best M. 2010. Trade-offs and responsiveness of the single-layer urban canopy parameterization in WRF: An offline evaluation using the MOSCEM optimization algorithm and field observations. *Q. J. R. Meteorol. Soc.* **136**: 997–1019. <https://doi.org/10.1002/qj.614>.
- Loridan T, Grimmond CSB, Offerle BD, Young DT, Smith TEL, Järvi L, Lindberg F. 2011. Local-scale Urban Meteorological Parameterization Scheme (LUMPS): Longwave radiation parameterization and seasonality-related developments. *J. Appl. Meteorol. Climatol.* **50**: 185–202. <https://doi.org/10.1175/2010JAMC2474.1>.
- Masson V. 2000. A physically based scheme for the urban energy budget in atmospheric models. *Boundary-Layer Meteorol.* **94**: 357–397. <https://doi.org/10.1023/A:1002463829265>.

- Masson V, Champeaux JL, Chauvin F, Meriguet C, Lacaze R. 2003. A global database of land surface parameters at 1 km resolution in meteorological and climate models. *J. Clim.* **16**: 1261–1282. <https://doi.org/10.1175/1520-0442-16.9.1261>.
- Masson V, Le Moigne P, Martin E, Faroux S, Alias A, Alkama R, Belamari S, Barbu A, Boone A, Bouyssel F, Brousseau P, Brun E, Calvet JC, Carrer D, Decharme B, Delire C, Dognon S, Essauoui K, Gibelin AL, Giordani H, Habets F, Jidane M, Kerdran G, Kourzeneva E, Lafaysse M, Lafort S, Lebeauvin Brossier C, Lemonsu A, Mahfouf J-F, Marguinaud P, Mokhtari M, Morin S, Pigeon G, Salgado R, Seity Y, Taillefer F, Tanguy G, Tulet P, Vincendon B, Vionnet V, Voldoire A. 2013. The SURFEXv7.2 land and ocean surface platform for coupled or offline simulation of earth surface variables and fluxes. *Geosci. Model Dev.* **6**: 929–960. <https://doi.org/10.5194/gmd-6-929-2013>.
- Miao C, Duan Q, Sun Q, Huang Y, Kong D, Yang T, Ye A, Di Z, Gong W. 2014. Assessment of CMIP5 climate models and projected temperature changes over Northern Eurasia. *Environ. Res. Lett.* **9**: 55. <https://doi.org/10.1088/1748-9326/9/5/055007>.
- Nakayama T, Fujita T. 2010. Cooling effect of water-holding pavements made of new materials on water and heat budgets in urban areas. *Landsc. Urban Plan.* **96**: 57–67. <https://doi.org/10.1016/j.landurbplan.2010.02.003>.
- Nordbo A, Karsisto P, Matikainen L, Wood CR, Järvi L. 2015. Urban surface cover determined with airborne lidar at 2 m resolution – Implications for surface energy balance modelling. *Urban Clim.* **13**: 52–72. <https://doi.org/10.1016/j.uclim.2015.05.004>.
- Offerle B, Grimmond CSB, Oke TR, Columbia B. 2003. Parametrization of net all-wave radiation for urban areas. *J. Appl. Meteorol.* **42**: 1157–1173.
- Oke TR. 1982. The energetic basis of the urban heat island. *Q. J. R. Meteorol. Soc.* **108**: 1–24. <https://doi.org/10.1002/qj.49710845502>.
- Oleson KW, Bonan GB, Feddema J, Vertenstein M. 2008a. An urban parameterization for a global climate model. Part II: Sensitivity to input parameters and the simulated urban heat island in offline simulations. *J. Appl. Meteorol. Climatol.* **47**: 1061–1076. <https://doi.org/10.1175/2007JAMC1598.1>.
- Oleson KW, Bonan GB, Feddema J, Vertenstein M, Grimmond CSB. 2008b. An urban parameterization for a global climate model. Part I: Formulation and evaluation or two cities. *J. Appl. Meteorol. Climatol.* **47**: 1038–1060. <https://doi.org/10.1175/2007JAMC1597.1>.
- Oleson KW, Bonan GB, Feddema J. 2010a. Effects of white roofs on urban temperature in a global climate model. *Geophys. Res. Lett.* **37**: L03701. <https://doi.org/10.1029/2009GL042194>.
- Oleson KW, Bonan GB, Feddema J, Vertenstein M, Kluzek E. 2010b. ‘Technical description of an urban parameterization for the Community Land Model (CLMU)’, Technical report NCAR/TN-480+STR. National Center for Atmospheric Research: Boulder, CO.
- Oleson KW, Monaghan A, Wilhelm O, Barlage M, Brunsell N, Feddema J, Hu L, Steinhoff DF. 2015. Interactions between urbanization, heat stress, and climate change. *Clim. Change* **129**: 525–541. <https://doi.org/10.1007/s10584-013-0936-8>.
- Parlow E, Vogt R, Feigenwinter C. 2014. The urban heat island of Basel seen from different perspectives. *Die Erde* **145**: 96–110. <https://doi.org/10.12854/erde-145-8>.
- Perkins SE, Pitman AJ, Holbrook NJ, McAneney J. 2007. Evaluation of the AR4 climate model’s simulated daily maximum temperature, minimum temperature, and precipitation over Australia using probability density functions. *J. Clim.* **20**: 4356–4376. <https://doi.org/10.1175/JCLI4253.1>.
- Phelan PE, Kaloush K, Miner M, Golden J, Phelan B, Silva H III, Taylor RA. 2015. Urban heat island: Mechanisms, implications, and possible remedies. *Annu. Rev. Environ. Resour.* **40**: 285–307. <https://doi.org/10.1146/annurev-environ-102014-021155>.
- Pielke RA. 2002. *Mesoscale Meteorological Modeling* (2nd edn). Academic Press: Cambridge, MA.
- Prein AF, Langhans W, Fossier G, Ferrone A, Ban N, Goergen K, Keller M, Tölle M, Gutjahr O, Feser F, Brisson E, Kollet S, Schmidli J, Van Lipzig NPM, Leung R. 2015. A review on regional convection-permitting climate modeling: Demonstrations, prospects, and challenges. *Rev. Geophys.* **53**: 323–361. <https://doi.org/10.1002/2014RG000475>.
- Quah AK, Roth M. 2012. Diurnal and weekly variation of anthropogenic heat emissions in a tropical city, Singapore. *Atmos. Environ.* **46**: 92–103. <https://doi.org/10.1016/j.atmosenv.2011.10.015>.
- Roth M. 2000. Review of atmospheric turbulence over cities. *Q. J. R. Meteorol. Soc.* **126**: 941–990. <https://doi.org/10.1256/smsqj.56408>.
- Roth M. 2007. Review of urban climate research in (sub)tropical regions. *Int. J. Climatol.* **27**: 1859–1873. <https://doi.org/10.1002/joc.1591>.
- Roth M, Jansson C, Velasco E. 2017. Multi-year energy balance and carbon dioxide fluxes over a residential neighbourhood in a tropical city. *Int. J. Climatol.* **37**(5): 2679–2698. <https://doi.org/10.1002/joc.4873>.
- Schneider A, Friedl MA, Potere D. 2010. Mapping global urban areas using MODIS 500-m data: New methods and datasets based on ‘urban ecoregions’. *Remote Sens. Environ.* **114**: 1733–1746. <https://doi.org/10.1016/j.rse.2010.03.003>.
- Schubert S, Grossman-Clarke S. 2012, Martilli A. A double-canyon radiation scheme for multi-layer urban canopy models. *Boundary-Layer Meteorol.* **145**: 439–468. <https://doi.org/10.1007/s10546-012-9728-3>.
- See L, Mills G, Ching J. 2015. Climate modelling: Community initiative tackles urban heat. *Nature*. **526**: <https://doi.org/10.1038/526043b>.
- Seto KC, Güneralp B, Hutya LR. 2012. Global forecasts of urban expansion to 2030 and direct impacts on biodiversity and carbon pools. *Proc. Natl. Acad. Sci. U.S.A.* **109**: 16083–16088. <https://doi.org/10.1073/pnas.1211658109>.
- Song J, Wang ZH. 2014. Interfacing the urban land atmosphere system through coupled urban canopy and atmospheric models. *Boundary-Layer Meteorol.* **154**: 427–448. <https://doi.org/10.1007/s10546-014-9980-9>.
- Starke P, Göbel P, Coldewey WG. 2010. Urban evaporation rates for water-permeable pavements. *Water Sci. Technol.* **62**: 1161–1169.
- Stewart ID, Oke TR. 2012. Local climate zones for urban temperature studies. *Bull. Am. Meteorol. Soc.* **93**: 1879–1900. <https://doi.org/10.1175/BAMS-D-11-00019.1>.
- Stocker TF, Qin D, Plattner G-K, Tignor MMB, Allen SK, Boschung J, Nauels A, Xia Y, Bex V, Midgley PM (eds). 2013. *Climate Change 2013: The Physical Science Basis. Contribution of Working Group I to the Fifth Assessment Report of the Intergovernmental Panel on Climate Change*. Cambridge University Press: Cambridge, UK and New York, NY.
- Taylor KE. 2001. Summarizing multiple aspects of model performance in a single diagram. *J. Geophys. Res.* **106**: 7183–7192. <https://doi.org/10.1029/2000JD900719>.
- Thiery W, Davin EL, Panitz HJ, Demuzere M, Lhermitte S, van Lipzig NPM. 2015. The impact of the African great lakes on the regional climate. *J. Clim.* **28**: 4061–4085. <https://doi.org/10.1175/JCLI-D-14-00565.1>.
- Thiery W, Davin EL, Seneviratne SI, Bedka K, Lhermitte S, van Lipzig NPM. 2016. Hazardous thunderstorm intensification over Lake Victoria. *Nature Commun.* **7**: 12786. <https://doi.org/10.1038/ncomms12786>.
- Tools for Sustainability. 2012. Autodesk Ecotect Analysis. Cal Poly Department of Architecture: Pomona, CA. <http://www.toolsforsustainability.com/index.php/component/content/article/9-reviews/software/412-autodesk-ecotect-analysis> (accessed 29 March 2017).
- Trusilova K, Früh B, Brien S, Walter A, Masson V, Pigeon G, Becker P. 2013. Implementation of an urban parameterization scheme into the regional climate model COSMO-CLM. *J. Appl. Meteorol. Climatol.* **52**: 2296–2311. <https://doi.org/10.1175/JAMC-D-12-0209.1>.
- Trusilova K, Schubert S, Wouters H, Früh B, Grossman-Clarke S, Demuzere M, Becker P. 2015. The urban land use in the COSMO-CLM model: A comparison of three parameterizations for Berlin. *Meteorol. Z.* **25**: 231–244. <https://doi.org/10.1127/metz/2015/0587>.
- Velasco E, Roth M. 2010. Cities as net sources of CO<sub>2</sub>: Review of atmospheric CO<sub>2</sub> exchange in urban environments measured by eddy covariance technique. *Geogr. Compass* **4**: 1238–1259. <https://doi.org/10.1111/j.1749-8198.2010.00384.x>.
- Velasco E, Roth M, Tan SH, Quak M, Nabarro SDA, Norford L. 2013. The role of vegetation in the CO<sub>2</sub> flux from a tropical urban neighbourhood. *Atmos. Chem. Phys.* **13**: 10185–10202. <https://doi.org/10.5194/acp-13-10185-2013.202>.
- Velasco E, Roth M, Norford L, Molina LT. 2016. Does urban vegetation enhance carbon sequestration? *Landsc. Urban Plan.* **148**: 99–107. <https://doi.org/10.1016/j.landurbplan.2015.12.003>.
- Wang ZH, Bou-Zeid E, Smith JA. 2013. A coupled energy transport and hydrological model for urban canopies evaluated using a wireless sensor network. *Q. J. R. Meteorol. Soc.* **139**: 1643–1657.
- Ward HC, Kotthaus S, Järvi L, Grimmond CSB. 2016. Surface Urban Energy and Water Balance Scheme (SUEWS): Development and evaluation at two UK sites. *Urban Clim.* **18**: 1–32.
- Watts N, Adger WN, Agnolucci P, Blackstock J, Byass P, Cai W, Chaytor S, Colbourn T, Collins M, Cooper A, Cox PM, Depledge J, Drummond P, Ekins P, Galaz V, Grace D, Graham H, Grubb M, Haines A, Hamilton I, Hunter A, Jiang X, Li M, Kelman I, Liang L, Lott M, Lowe R, Luo Y, Mace G, Maslin M, Nilsson M, Oreszczyn T, Pye S, Quinn T, Svendsdotter M, Venevsky S, Warner K, Xu B, Yang J, Yin Y, Yu C, Zhang Q, Gong P, Montgomery H, Costello A. 2015. Health and climate change: Policy responses to protect public health. *Lancet* **386**: 1861–1914. <https://doi.org/10.1016/S0140-6736>.
- Willmott CJ, Matsuura K. 2005. Advantages of the mean absolute error (MAE) over the root mean square error (RMSE) in assessing average model performance. *Clim. Res.* **30**: 79–82.
- Wouters H, De Ridder K, van Lipzig NP. 2012. Comprehensive parameterization of surface-layer transfer coefficients for use in atmospheric numerical models. *Boundary-Layer Meteorol.* **145**: 539–550. <https://doi.org/10.1007/s10546-012-9744-3>.
- Wouters H, Demuzere M, Ridder KD, Nicole PM. 2015. The impact of impervious water-storage parameterization on urban climate modelling. *Urban Clim.* **11**: 24–50. <https://doi.org/10.1016/j.uclim.2014.11.005>.
- Wouters H, Demuzere M, Blahak U, Fortuniak K, Mahieu B, Camps J, Tielemans D, van Lipzig NP. 2016. Efficient urban canopy parameterization for atmospheric modelling: Description and application with the COSMO-CLM model (version 5.0.clm6) for a Belgian summer. *Geosci. Model Dev.* **9**: 3027–3054. <https://doi.org/10.5194/gmd-9-3027-2016>.
- Xu W, Wooster MJ, Grimmond CSB. 2008. Modelling of urban sensible heat flux at multiple spatial scales: A demonstration using airborne hyperspectral imagery of Shanghai and a temperature-emissivity separation approach. *Remote Sens. Environ.* **112**: 3493–3510. <https://doi.org/10.1016/j.rse.2008.04.009>.
- Zhao L, Lee X, Smith RB, Oleson K. 2014. Strong contributions of local background climate to urban heat islands. *Nature* **511**: 216–219. <https://doi.org/10.1038/nature13462>.